International Journal of Coal Geology 272 (2023) 104253

Contents lists available at ScienceDirect

International Journal of Coal Geology

journal homepage: www.elsevier.com/locate/coal

Silurian black shales from Sousel-Barrancos Metallogenic Belt (Ossa-Morena Zone, Portugal): Characterization and interplay to Cu deposits

V. Laranjeira [a,*], J. Ribeiro [b], N. Moreira [c], P. Nogueira [d], J.G. Mendonça Filho [e], F. Rocha [f], D. Flores [a]

[a] Institute of Earth Sciences, Pole of University of Porto and University of Porto, Department of Geosciences, Environment and Spatial Planning, Rua do Campo Alegre, 4169-007 Porto, Portugal
[b] University of Coimbra, Instituto Dom Luiz, Department of Earth Sciences, Rua Sílvio Lima, 3030-790 Coimbra, Portugal
[c] Institute of Earth Sciences, Pole of University of Évora, Department of Geosciences and Instituto de Investigação e Formação Avançada (IIFA), University of Évora, Colégio Luís António Verney, Rua Romão Ramalho, 59, 7000-671 Évora, Portugal
[d] Institute of Earth Sciences, Pole of University of Évora and University of Évora, Department of Geosciences, Colégio Luís António Verney, Rua Romão Ramalho, 59, 7000-671 Évora, Portugal
[e] Laboratory of Palynofacies and Organic Facies (LAFO), Department of Geology, Institute of Geosciences, Federal University of Rio de Janeiro, Brazil
[f] Department of Geosciences, GeoBioTec, University of Aveiro. Campus Universitário de Santiago, 3810-193 Aveiro, Portugal

ARTICLE INFO

Keywords:
Organic matter
Thermal maturation
Paleotemperature
Geochemical composition
Redox sensitive elements
Mineralization processes

ABSTRACT

Black shales are commonly spatially associated with metal-rich deposits, wherein organic matter in these rocks may condition or influence the processes related with the concentration of metals and formation of ore deposits. In the Ossa-Morena Zone (South of Portugal), namely in the Sousel-Barrancos metallogenic belt, several Cu mineralized veins occurs, being generally hosted in Silurian metasedimentary units mainly composed of black and grey shales, with interbedded lyddites and black quartzites. This research aims to contribute to the study of the association between those Silurian black shales and the Cu ore deposition in the Sousel-Barrancos metallogenic belt. The petrographic, geochemical and mineralogical analysis of black shales was performed to characterize the organic and inorganic fractions, to investigate elements concentration and its mode of occurrence. The data allow to identify the spatial pattern of thermal maturation of these black shales related to the variability of metamorphic processes, and the studied samples collected in drill cores from Miguel Vacas deposit also allow to identify an irregular pattern of maturation associated to the pathway of hydrothermal fluids. A significant Cu enrichment in black shales in the supergene enrichment domains were identified and data seems to indicate that Cu concentration is not directly related with organic carbon content, probably indicating a distinct source for Cu content. The mobilization of hydrothermal fluids, possibly of magmatic source, contributed to the discrepant maturation of organic matter in black shales.

1. Introduction

Black shales are being investigated worldwide because their relation with hydrocarbon generation, as well as spatial association with several metal deposits (e.g., Au, Ag, Co, Cu, Hg, Mo, Ni, Mn, Sb, V, U, Zn, W, PGE and others) (e.g., Vine and Tourtelot, 1970; Wignall, 1994; Coveney and Pašava, 2004). Numerous metal-rich deposits are related with host rocks that have a high concentration of organic carbon, such as black shales, suggesting that organic matter is somehow implicated with the metallogenic mechanisms, playing a role in the deposition and concentration of metals. Another hypothesis is that the rocks are themselves a source of metals that can be remobilized and concentrated elsewhere (Leventhal, 1986; Maynard et al., 2001; Coveney and Pašava, 2004; Greenwood et al., 2013; Wang et al., 2022).

* Corresponding author at: Institute of Earth Sciences, Pole of University of Porto and University of Porto, Department of Geosciences, Environment and Spatial Planning, Rua do Campo Alegre, 4169-007 Porto, Portugal.
E-mail addresses: vanessa.laranjeira@fc.up.pt (V. Laranjeira), joana.ribeiro@uc.pt (J. Ribeiro), nafm@uevora.pt (N. Moreira), pmn@uevora.pt (P. Nogueira), graciano@geologia.ufrj.br (J.G. Mendonça Filho), tavares.rocha@ua.pt (F. Rocha), dflores@fc.up.pt (D. Flores).

https://doi.org/10.1016/j.coal.2023.104253
Received 21 February 2023; Received in revised form 10 April 2023; Accepted 1 May 2023
Available online 2 May 2023

Usually, metals are transported in hydrothermal fluids to a location where deposition occurs, as response to physicochemical variations of the environment or of the fluid itself (Meyers et al., 1992). The metallic enrichment can result from redox reactions facilitated by bacteria during early diagenesis and can also be associated with post-diagenetic hydrothermal processes after deep burial evolution (Meyers et al., 1992). The continued inflow of metal bearing solutions can lead to the deposition of substantial amounts of metalliferous minerals, and, in favorable conditions, this enrichment generates ore deposits (Meyers et al., 1992).

The organic matter may have an active role in numerous processes related with the ore deposits genesis: transportation, mobilization, deposition, concentration, reduction, and preservation (e.g., Leventhal, 1986, 1993; Meyers et al., 1992; Suárez-Ruiz et al., 2012). Mossman (1999) confirmed that the organic matter may concentrate metals through accumulation in living organisms (biomineralization processes), metal absorption, and organic matter facilitation of reduction reactions through electron donation (Suárez-Ruiz et al., 2012). Organic matter interacts with metals due to their inherent reducing, acidic and chelating properties (e.g., Disnar and Sureau, 1990; Mossman, 1999). The redox reactions are important in diagenetic and epigenetic ore forming environments wherein organic matter acts as a reducing agent for soluble metal sulfates in the generation of metal-sulfide deposits and/or the reduction of soluble metal cations to the insoluble native element (e.g., Disnar and Sureau, 1990; Mossman, 1999; Suárez-Ruiz et al., 2012).

The study of organic matter in rocks can be used to understand the metallic ore concentration and, consequently, the processes related with ore deposits genesis (Suárez-Ruiz et al., 2012). The detailed characterization of the organic matter supports the evaluation of the time-temperature history either in ores or host rocks, once reflectance of the organic particles increases with thermal maturation through burial, hydrothermal or magmatic activity (e.g., Eakin and Gize, 1992; Landais, 1993; Macqueen, 1984 *in* Suárez-Ruiz et al., 2012). These studies also reveal the active or passive role that organic matter plays in ore formation, thereby helping to discuss or even determine the source of metals, transportation, and precipitation mechanisms (Suárez-Ruiz et al., 2012). Key parameters to be analyzed in the organic matter occurring in association with ore deposits are the source and type of organic matter, its thermal evolution (maturation) and spatial variation, hence, identifying possible thermal anomalies (Gize, 1993; Suárez-Ruiz et al., 2012). These parameters can be assessed by petrographic techniques, including the analysis of the reflectance of organic matter, that is useful to estimate paleotemperatures. Vitrinite reflectance is widely used, being a robust thermal maturity parameter (Tissot and Welte, 1984; Hunt, 1996; Hackley et al., 2009). However, Pre-Devonian rocks do not contain vitrinite, because it is originated from vascular land plants that postdated the Late Silurian times (Tissot and Welte, 1984; Taylor et al., 1998); nevertheless, the reflectance of other organic components, namely faunal remains, are used to quantify the thermal maturation of sequences of this age (Hartkopf-Fröder et al., 2015).

The combination of organic petrographic methods with geochemical analysis allows the characterization of the source, type and maturation of organic matter, and to identify the active or passive role in the concentration of metals in a specific ore deposit (Suárez-Ruiz et al., 2012). The geochemical analysis of organic and inorganic fractions provides further information on elements concentration, depositional environment, migration pathways of hydrothermal fluids and can contribute to the knowledge of mineralization processes (Tissot and Welte, 1984; Peters et al., 2005; Greenwood et al., 2013).

This research aims to explore the relationship between Silurian black shales and the spatially associated Cu mineralizations, with a focus on the role of organic matter in the ore forming processes of the Ossa-Morena Zone (OMZ), Portugal. For this, the specific objectives are: identify type, source, and maturation of the organic matter by petrographic analyses; and, determine the geochemical composition of black shales to explore elements concentration, mode of occurrence and paleodepositional conditions of the Silurian black shales.

2. Geological setting

The OMZ is a tectonostratigraphic zone of the Iberian Massif (Fig. 1A), showing differentiated stratigraphic, magmatic, and structural features (e.g., Ribeiro et al., 2007; Moreira et al., 2014; Quesada and Oliveira, 2019). The complex and multicycle evolution of this zone is also recorded in its metallogenic features, generating several small-scale ore deposits, including *syn*-sedimentary, syn-metamorphic and syn-magmatic deposits controlled either by Cadomian or Variscan cycles (Tornos et al., 2004; Mateus et al., 2013): base metal-bearing veins, polymetallic massive sulfide deposits, Fe-skarns, magnetite and Cu—Ni magmatic ore bodies, among others. The spatial disposition and the metallogenic models of those mineralizations allowed to discriminate several metallogenic belts in the OMZ (Fig. 1B).

In central OMZ, namely in Sousel-Barrancos metallogenic belt, several Cu—Fe (±Zn ± Pb ± Au) vein occurrences and deposits are known, that share common features. The Cu—Fe veins are composed of quartz-carbonate and sulfides, being hosted in Paleozoic metasedimentary series (Mateus et al., 2003, 2013; Maia et al., 2019, 2020). Several of these Cu—Fe veins were object of exploitation, during the 19th and 20th centuries (e.g., Oliveira, 1984, 1986; Matos and Rosa, 2001; Mateus et al., 2003, 2013; Tornos et al., 2004). In the Sousel-Barrancos belt, there are two important clusters of Cu occurrences (Fig. 1B and C): (1) Alandroal cluster, where the Bugalho, Zambujeira, Miguel Vacas and Mociços (Fig. 2A) mines are located, and (2) Barrancos cluster, where the Minancos, Aparis, Botefa and Defesa das Mercês mines are placed (Fig. 2B) (Matos and Filipe, 2013; Mateus et al., 2013).

Those fault-controlled Cu veins were developed along several trends, being described NNW-SSE, NNE-SSW and ENE-WSW veins, being also developed along the NW-SE regional trend. These structures comprise polyphase, brechified hydrothermal fills, composed of quartz, carbonates (dolomite, ankerite, siderite and calcite), sulfides (chalcopyrite, pyrite, arsenopyrite, sphalerite, pyrrhotite and galena) and sulfosalt minerals (tetrahedrite-tenantite) (Mateus et al., 2013). Supergenic enrichment processes are also common, leading to the development of mineral associations consisting of iron (hidr-)oxides, malachite and azurite, cuprite and other secondary Cu minerals (Mateus et al., 2013).

As aforementioned, the veins cut the Paleozoic metasedimentary successions, namely Ordovician to Lower Devonian units (Fig. 2B). Nevertheless, most of veins are hosted in black to grey shales, sometimes with interbedded lydites and black quartzites (Oliveira, 1986; Mateus et al., 2013) of Silurian to Lower Devonian age (*Xistos com Nódulos* and *Xistos Raiados* Formations; Fig. 1). The presence of disseminated sulfides is also a common feature on the Silurian black shales (Oliveira, 1986).

As respect to the genesis of these veins, it is considered that mineralized structures are related with hydrothermal activity contemporaneous of late Variscan brittle deformation stages (Oliveira, 1984; Mateus et al., 2003, 2013; Maia et al., 2019, 2020). According to some authors (Oliveira, 1986; Mateus et al., 2003, 2013; Tornos et al., 2004), the Cu content is considered to be a result of remobilization from the metasedimentary succession, specifically from the Silurian succession which contains organic matter deposited in euxinic conditions (Piçarra, 2000; Araújo et al., 2013; Roseiro et al., 2020). Other authors (Tornos et al., 2004; Mateus et al., 2013) also emphasizes the presence of anomalous Au concentration in some those Cu dykes (Defesa das Mercês and Mostardeira), discussing a possible volcanogenic primary source of metals. Recently, Maia et al. (2020) highlights the presence of magmatic-hydrothermal derived fluids related with Cu vein deposits in Sousel-Barrancos metallogenic belt. The authors hypothesized the existence of a deep-seated magmatic body as possible source of hydrothermal fluids (and metals?), however not excluding the possibility that Paleozoic metasedimentary units contributed as a metal source for ore deposits.

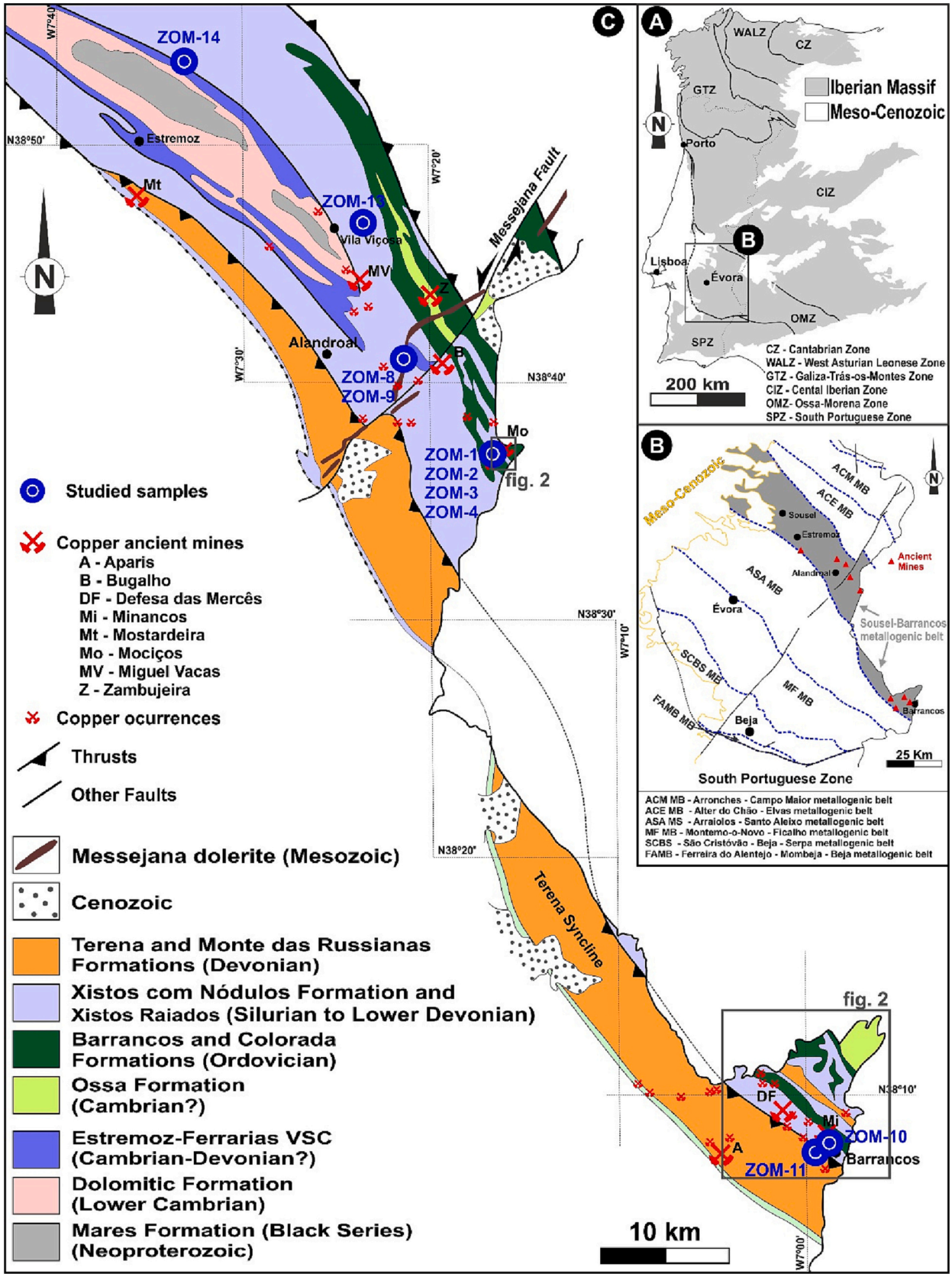

Fig. 1. A) OMZ localization on Iberian Massif context (LNEG, 2010); B) Representation of the different metallogenic zones of OMZ (adapted from Oliveira, 1986; Mateus et al., 2013); C) Location of Cu mines and occurrences in the Sousel-Barrancos Metallogenic Belt (adapted from Matos and Filipe, 2013).

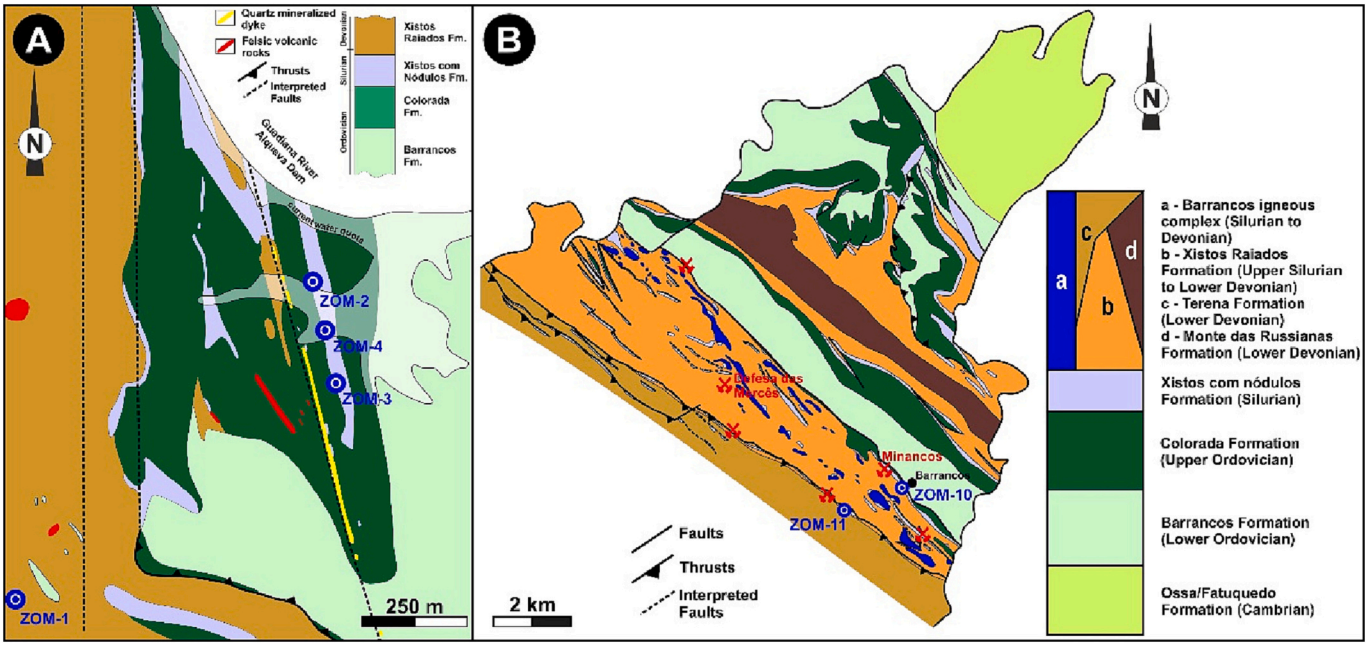

Fig. 2. A) Geological map of the Mociços mine (adapted from maps of the Serviço de Fomento Mineiro, Vitor Oliveira); B) Geological map of the Barrancos region with the location of the Minancos mine (adapted from Piçarra, 2000 and Araújo et al., 2013).

3. The Miguel Vacas Cu vein case study

In the Sousel-Barrancos metallogenic belt there are several Cu-rich vein ancient mines (e.g., Mociços or Miguel Vacas) and occurrences (e.g., Ferrarias). The Miguel Vacas mine, located in the Alandroal cluster (5 km SE from Vila Viçosa - district of Évora; Fig. 1C), is an ancient mine that was exploited as an open pit, but in the initial phase was exploited underground (Fig. 3A, B and C). The mining activities lasted between 1925 and 1986 (Fernandes, 2012).

The Miguel Vacas mine exploited an array of Cu veins that occur in the NE limb of the Estremoz Anticline (Fig. 1), being hosted in the Silurian metasedimentary succession (Fig. 4; *Xistos com Nódulos* Formation), mainly composed of black to grey shales (Oliveira, 1986; Tornos et al., 2004; Corrula and Branco, 2005; Mateus et al., 2013), with low grade metamorphism, not exceeding the greenschist facies in the chlorite-biotite zones (Oliveira, 1984; Pereira et al., 2012; Moreira et al., 2019). It is an anastomosing vein structure that extends over 2000 m in length, with an NNW-SSE direction, and dipping 50° - 80° to E, presenting variable thickness between 10 and 20 m (Corrula and Branco, 2005; Fernandes, 2012). The Miguel Vacas Cu vein is mostly composed

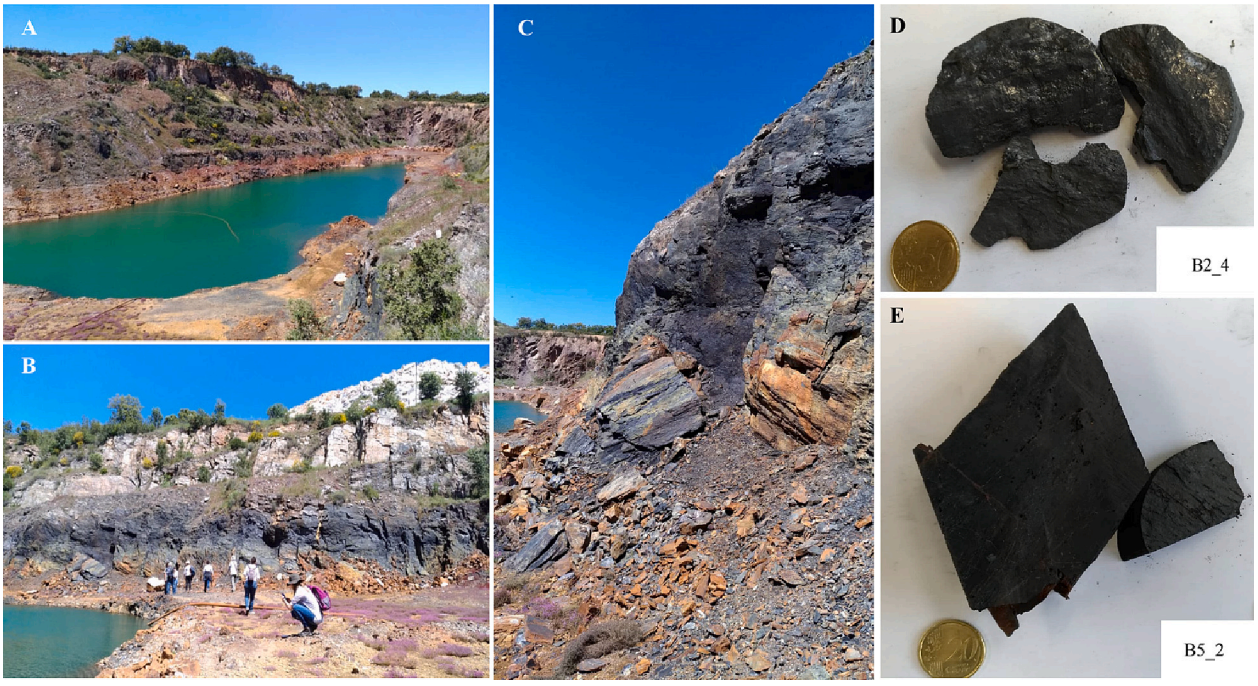

Fig. 3. A) Miguel Vacas open pit mine; B) and C) Miguel Vacas outcrops with visible black shales; D) and E) Examples of samples selected from drill cores of boreholes executed in Miguel Vacas area.

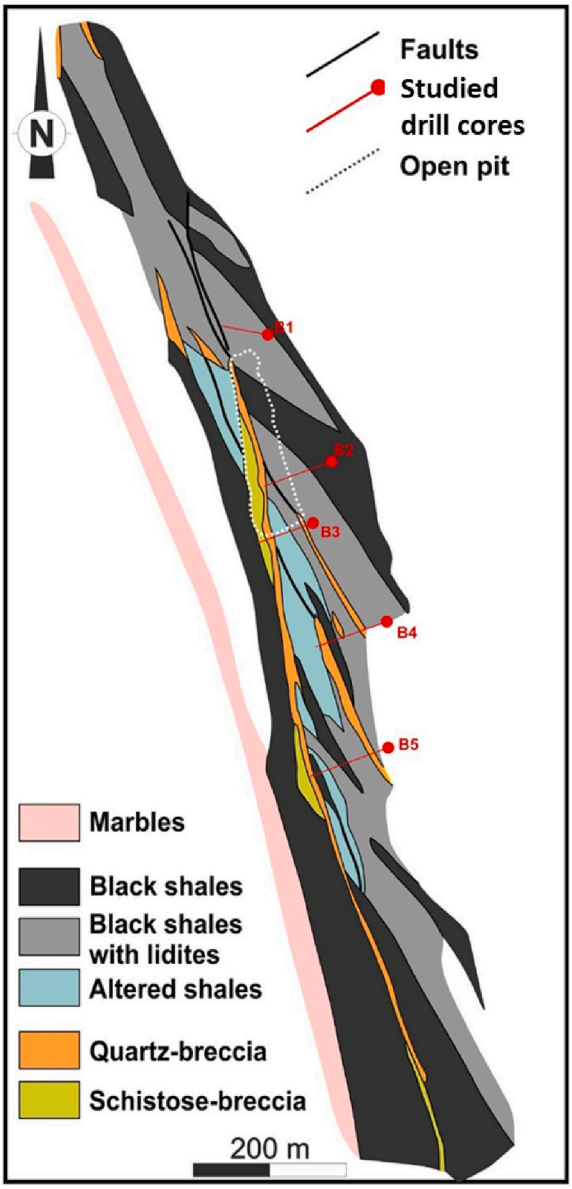

Fig. 4. Geological map of the Miguel Vacas deposit and location of the boreholes (adapted from Corrula and Branco, 2005).

of fault breccias, including heterometric, angular and hydrothermally altered fragments of diverse shale host rocks, and quartz breccias (Fig. 4; Mateus et al., 2003; Fernandes, 2012).

Prospecting works carried out during the 20th century, recognize the mineralization until 330 m in depth and the first 80–90 m corresponding to a horizon of supergene metal-enrichment, being the primary Cu sulfides mineralization at higher depths (Mateus et al., 2003; Fernandes, 2012).

The primary ore (deepest zone) is mainly composed of sulfides (chalcopyrite, pyrite and arsenopyrite) associated with fault breccias containing quartz and carbonates (cal ± ank ± sd) (Mateus et al., 2003, 2013; Fernandes, 2012). In contrast, the supergenic enrichment domain (superficial zone), which results from a horizon where a strong oxidation and hydration occurred, is composed of a combination of secondary Cu minerals such as, carbonates (malachite and azurite), phosphates (libethenite and pseudomalachite), sulfates (brochantite), sulfides (cuprite, chalcocite, bornite, covellite) and native Cu, associated with some Bi mineral phases (Fernandes, 2012).

Beyond the significant Cu content, Miguel Vacas veins also show a significant content of Au (Mateus et al., 2003), although occurs erratically throughout the profile, probably because it occurs as micro-inclusions both in the primary and secondary sulfide phases (Fernandes, 2012).

4. Sampling and methodology

A total of 39 samples of Silurian black shales from Sousel-Barrancos metallogenic belt were studied: 10 from outcrops and 29 from drill cores. Samples from drill cores were collected in five boreholes performed by a private company for exploration in the Miguel Vacas Cu deposit during 2014 and 2015, being selected from different depths. The outcrop samples of black shales were mainly collected in Alandroal region (8 samples). From these, 4 samples were collected in outcrops near Mociços ancient mine and 2 samples near the Ferrarias occurrence. Other 2 outcrop samples were collected in Barrancos region, far from Cu occurrences. The samples collected far from the mineralizations may provide information from the background of the Sousel-Barrancos metallogenic belt Silurian black shales without the influence of mineralizing processes. Table 1 shows supplementary information about the collected samples.

During sampling in the outcrops, the superficial layers have been removed to avoid weathered material. The boreholes executed in Miguel Vacas mine area (Fig. 4) allow sampling along the drill cores, being selected fragments of black shales from different depths without evidences of weathering (Fig. 3D and E). Fig. 5 presents the logging details adapted from the information provided by the company. The proximity to mineralized veins was considered in the samples selection, in accordance with the logging information. The samples considered proximal to mineralized veins are located up to a maximum of 10 m from the mineralized veins (Fig. 5).

In the laboratory, the samples were dried and a representative rock fragment of about 30 to 40 mm^2 of each sample was selected for petrographic observations. Then the samples were crushed to 1 mm, homogenized, and quartered to get representative portions for petrographic studies, and crushed to 212 μm for geochemical analysis.

Polished blocks for petrographic analysis were done with both, the rock fragments, and the crushed samples in accordance with ISO standard (ISO 7404-2, 2009). The petrographic characterization through optical microscopy allowed the identification and characterization of the organic matter and the measurement of random and maximum reflectance of organic particles. The random and maximum reflectance (R_r and R_{max}, respectively) were measured following the ASTM D7708–14 (2014) standard. This standardized protocol refers that at least 20–30 particles should be measured; however, in some of the studied samples, it was not possible to find the minimum number of organic particles. The polished blocks of the solid pieces were useful to

Table 1
Systematization of sampling information.

Region	Samples
Alandroal - Mociços (outcrops)	ZOM 1, ZOM 2, ZOM 3, ZOM 4 (near the mineralization)
Alandroal - Ferrarias (outcrops)	ZOM 8, ZOM 9 (near the mineralization)
Alandroal (outcrops)	ZOM 13, ZOM 14 (far from the mineralization)
Alandroal - Miguel Vacas (drill cores)	B1 (84.1 m depth, 45° inclination): 5 samples (B1_1 to B1_5) B2 (144 m depth, 50° inclination): 6 samples (B2_1 to B2_6) B3 (109 m depth, 45° inclination): 5 samples (B3_1 to B3_5) B4 (195 m depth, 60° inclination): 6 samples B4_1 to B4_6) B5 (152 m depth, 45° inclination): 7samples (B5_1 to B5_7)
Barrancos (outcrops)	ZOM 10, ZOM 11 (far from the mineralization)

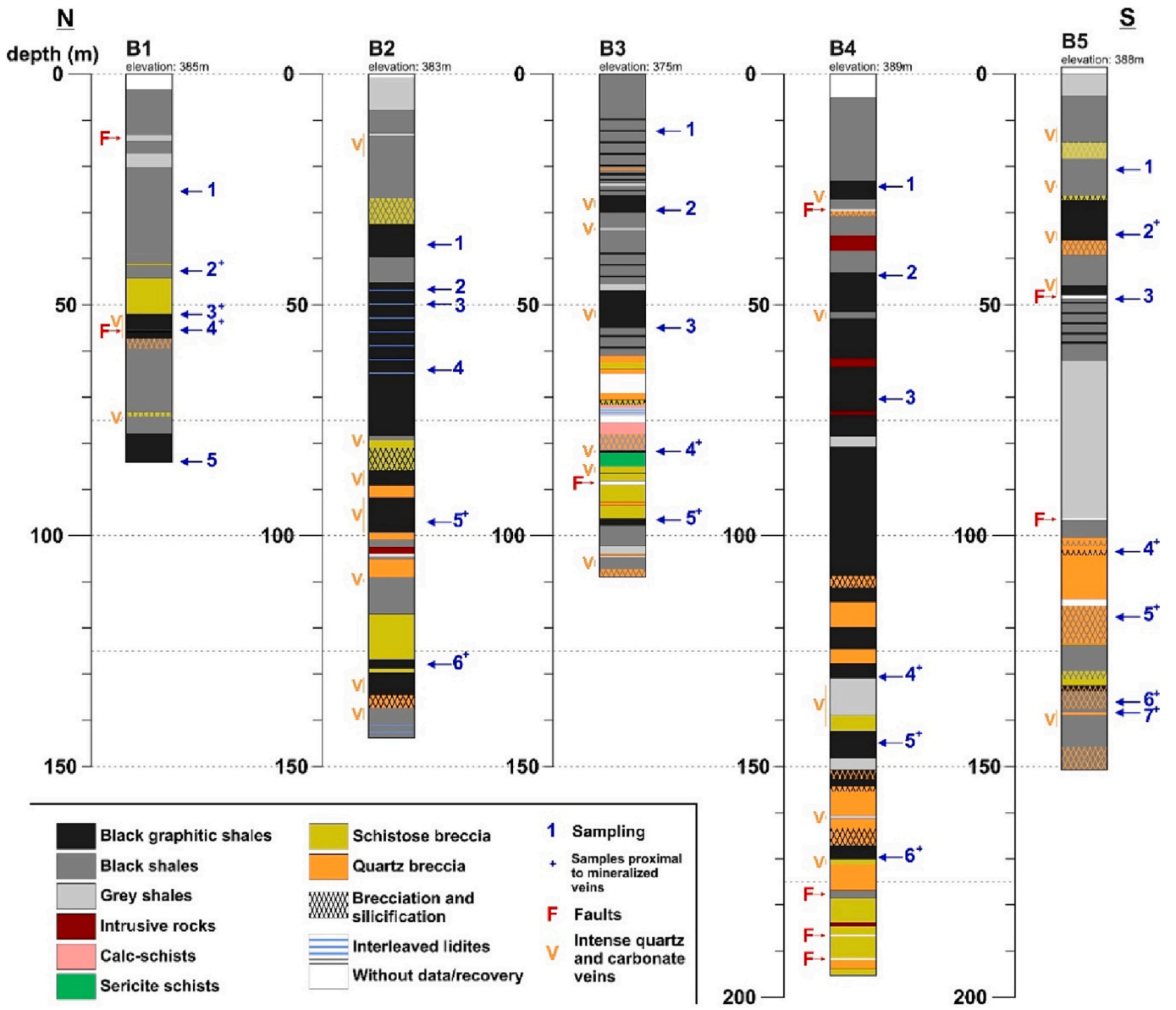

Fig. 5. Geological logging of the boreholes and identification of selected black shale samples for study (samples proximal to mineralized veins are marked in this figure and in the manuscript with the symbol +).

identify the association and modes of occurrence of the petrographic components, which may not be observable after crushing, and provide support for the interpretation of mineralogical and geochemical data. The petrographic observations and measurements were carried out using a Leica 4000 M microscope equipped with a Discus-Fossil system with immersion oil objective.

The geochemical characterization included the determination of total organic carbon (TOC) using a LECO SC 144 analyzer after samples acidification, following NCEA-C-1282, EMASC-001 (US - EPA, 2002) standard. The TOC and TS were determined in Laboratory of Palinofacies and Organic Facies (Federal University of Rio de Janeiro, Brazil). The concentration of major, minor and trace elements was determined using inductively coupled plasma emission spectrometry/mass spectrometry (ICP-ES/MS) after digestion with an acid solution of H_2O-HF-$HClO_4$-HNO_3, in Bureau Veritas Mineral Laboratories (Canada). Analysis of reference materials, duplicates and blanks was performed for quality assurance.

In selected samples, the X-Ray Diffraction (XRD) analysis was accomplished to support the mineral identification. The mineralogical composition was established by XRD with Cu-Kα radiation, using a Malvern Panalytical Phillips X'Pert PW3040/60 equipped with X´Pert 2.0 and Profit software at the Central Analysis Laboratory of the Department of Geosciences in the University of Aveiro (Portugal).

Scanning electron microscopy with energy dispersive X-ray spectrometry (SEM-EDX) analyses were also performed in selected samples to investigate the mineralogical constituents based on qualitative chemical compositions and the elements mode of occurrence. The observations under secondary electrons and back scattered electrons detection modes on the polished blocks were performed with an FEI Quanta 400FEG environmental SEM, equipped with a Genesis X4M energy dispersive X-ray analyzer in Materials Centre of the University of Oporto (Portugal).

The chemical composition of the studied black shales was compared with reference values reported for Background of Black Shales (BBS) (Ketris and Yudovich, 2009). The enrichment/depletion behavior of elements was determined relatively to the reference values (BBS) through calculation of concentration coefficients (CC). The Pearson correlation coefficients were calculated to investigate elements affinity,

supporting the identification of modes of occurrence. The ratio between redox sensitive elements were calculated to obtain information regarding depositional conditions and differences among the studied black shales (e.g., Hatch and Leventhal, 1992; Jones and Manning, 1994; Rimmer, 2004; Tribovillard et al., 2006; Ross and Bustin, 2009).

5. Results

5.1. Petrographic characterization of organic and inorganic matter

5.1.1. Alandroal and Barrancos outcrop samples

The petrographic observations of the Silurian black shales allowed the identification of vitrinite-like particles in all samples, all of them without evidence of weathering. The organic particles are generally thin and elongated, occurring, essentially, interbedded in the mineral matter (Fig. 6, 7 and 8). Organic particles are more abundant in sample ZOM 2, from the Alandroal area, and in sample ZOM 10, in the Barrancos area.

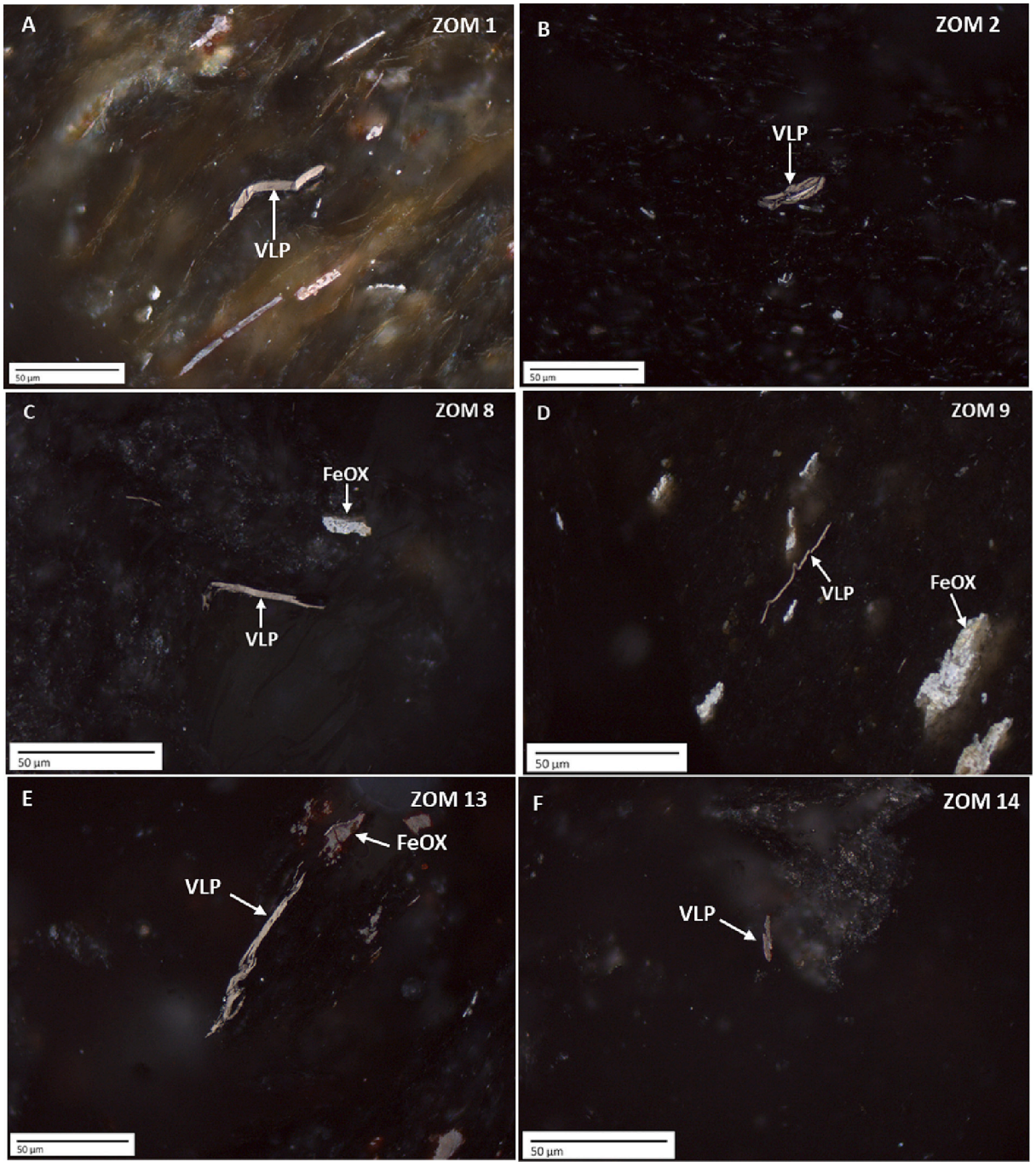

Fig. 6. Photomicrographs of the studied samples from: A) and B) Alandroal area near the mineralization exhibiting vitrinite-like particles (VLP) showing single flakes graphitic characteristics and iron oxides (FeOX), occurring within mineral matter; C) and D) Alandroal area near the mineralization exhibiting vitrinite-like particles (VLP) thin and elongated, essentially isolated, and some iron oxides (FeOX) particles; and E) and F) Alandroal area far from the mineralization exhibiting vitrinite-like particles (VLP) displaying single flakes graphitic features and iron oxides (FeOX).

In some samples from Alandroal area, near mineralized areas (ZOM 1, ZOM 2, ZOM 3, ZOM 4, ZOM 8 and ZOM 9) and the ones far from mineralization (ZOM 13 and ZOM 14), were observed vitrinite-like particles exhibiting single flakes graphitic features (Fig. 6A to 6F).

Some undifferentiated zooclasts were identified in samples ZOM 3 and ZOM 4 (Fig. 7A and 7B). The organic matter can be classified as zooclasts when some distinguished specific morphological characteristics are observed, e.g., fish spines and scales, arthropod exoskeletal debris, insect cuticles fragments, organic linings from bivalve shells, ostracod carapaces, graptolite fragments or crustacean eggs (Mendonça Filho and Gonçalves, 2017).

In samples from Barrancos (ZOM 10 and ZOM 11), remains of graptolites were identified (Figs. 7C to 7F). Graptolites are organic fossils that occur mainly in Lower Paleozoic (from Ordovician to Lower Devonian) (Goodarzi, 1984, 1985; Goodarzi and Norford, 1987), being abundant in black shales, siliceous shales and cherts, and are characteristic of external shelf to deep ocean environments (Cooper et al., 2012). Petrographically, under reflected light, graptolites can be distinguished by their characteristics, such as granularity, fusellar layer, anisotropy (Goodarzi, 1984, 1985; Goodarzi and Norford, 1987; Petersen et al., 2013; Luo et al., 2016; Gonçalves et al., 2020) and can show two different types of texture:

- Granular texture - graptolites show a fine granular to reticular form, are anisotropic (Goodarzi, 1984; Goodarzi et al., 1992; Gonçalves et al., 2020) and can be found mainly in carbonates (Goodarzi, 1984; Goodarzi and Norford, 1987; Petersen et al., 2013).
- Non-granular texture - it was described as presenting higher reflectance, strong anisotropy and are more common in shales (Goodarzi,

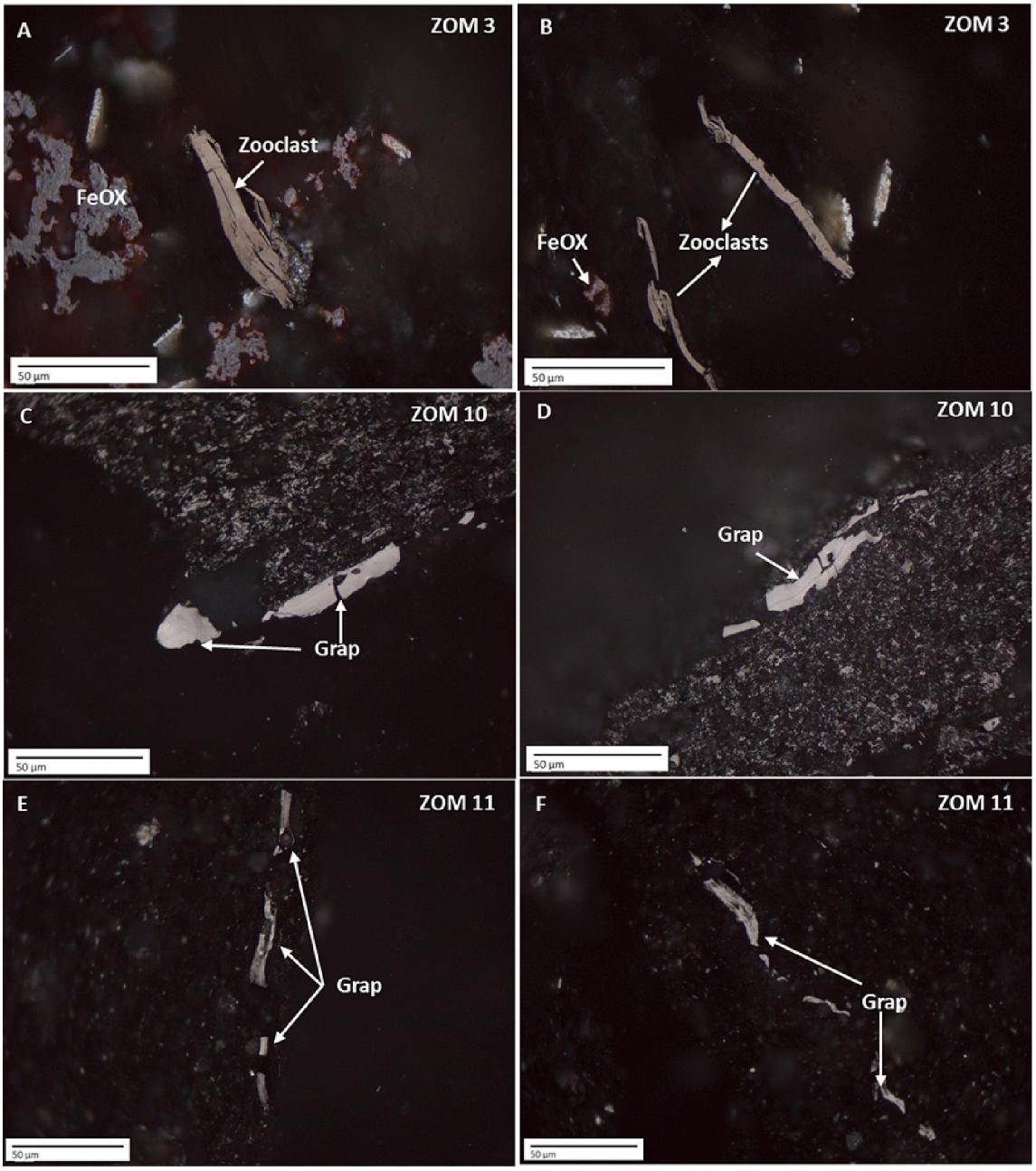

Fig. 7. A) and B) Photomicrographs of the samples from Alandroal area near the mineralization presenting fragments of zooclasts and iron oxides (FeOX) particles; C), D), E) and F) Photomicrographs of the samples from Barrancos displaying graptolites (Grap).

1984; Goodarzi and Norford, 1987; Petersen et al., 2013; Gonçalves et al., 2020).

In samples from Barrancos (ZOM 10 and ZOM 11), the fragments of graptolites are large compared to other organic particles, showing an elongated rectangular shape and usually presenting segmentation (Fig. 7D and 7E). Fragments of graptolites show a higher reflectance and anisotropy than other particles of organic matter, being possible to identify the non-granular texture. The abundance of graptolites in Barrancos area had already been noted (Piçarra, 2000).

The petrographic analysis also allows the observation of detrital silicate minerals occurring in association with organic matter. In Alandroal samples collected near Cu occurrences, the mineral matter is different among the studied samples: in ZOM 1, ZOM 3 and ZOM 8 is possible to observe abundant iron oxides (Fig. 6A, 6C, 7A and 8A), in ZOM 4 the presence of sulfides is noticeable, and in ZOM 2 and ZOM 9 a more siliceous material is noted. Otherwise, the samples collected in the Alandroal area, far from Cu occurrences, show more siliceous components in ZOM 14 (Fig. 8B) and the noticeable presence of iron oxides on ZOM 13 (Fig. 6E). Samples from Barrancos (ZOM 10 and ZOM 11) show a significant difference compared with others; they have less iron oxides and consist essentially of aluminosilicates and organic matter (Fig. 7C to 7F).

5.1.2. Miguel Vacas occurrence

Samples from Miguel Vacas allow to identify vitrinite-like particles in all samples, and generally they are thin and small in size, with varied morphology, and occur interbedded with mineral matter (Fig. 9A, B and C). Larger organic particles exhibiting graphitic structures are also observed in some samples, occurring as single flakes disseminated in fragments of interbedded mineral and organic matter (Fig. 9D, E and F). Additionally, graptolites (Figs. 10A to 10F) are also present in some samples; the fragments of graptolites found in samples B2_2, B2_3, B3_1, B3_2, and B5_2 are large compared to vitrinite-like particles, show an elongated rectangular shape and are segmented. They are interbedded with mineral matter, present non-granular texture and strong anisotropy.

It was possible to observe some differences in the mode of occurrence of organic matter between the different drill cores. In B1 the presence of particles exhibiting graphitic structures is more significant (Fig. 9D and E). In B2 were identified fragments of graptolites in two samples (B2_2 and B2_3) and, in general, the organic matter also occurs in massive particles interbedded with mineral matter (Fig. 9A). In samples from B3 and B4 drill cores, the organic matter is very similar, also occurring in larger massive particles with thin organic matter embedded with minerals (Fig. 9C). Graptolites are observed in samples B3_1 and B3_2 (Figs. 10C, 10D and 10E), while in the B4 were not identified. Samples from B5 have the lowest amount of organic particles when compared with the other drill cores; fragments of graptolites were observed in one sample (B5_2) (Fig. 10F).

The inorganic fraction is essentially composed of detrital derived minerals (mainly silicate minerals) and the presence of iron oxides is common (Fig. 11). In samples from drill cores B1 and B3, there is a greater presence of iron oxides when compared to the samples from the other drill cores (Fig. 11A; Fig. 12A), while samples from B2 and B5 presents more siliceous components (Fig. 12B). Samples from B4 stand out due to the presence of abundant sulfides, mainly in samples located near to the mineralized veins (Fig. 12C and D).

5.2. Mineralogical analysis

The XRD analysis was done in 4 outcrop samples (ZOM 3, ZOM 8, ZOM 13 and ZOM 10) and in 2 drill core samples (B4_3 and B4_6). The complete results are summarized in the supplementary materials (Table S1). The analysis allowed the identification of quartz, plagioclase and muscovite as major mineral phases in all samples, corroborating the petrographic observations, which shows that detrital silicate minerals are the main components. Chlorite, siderite and rutile are also identified in the analyzed samples. It was also detected arsenopyrite in most of samples (except in sample B4_3), pyrite in the drill core samples and malachite in samples ZOM 3, ZOM 8, ZOM 10, and B4_3.

The SEM-EDX analysis was performed in selected samples (ZOM 3, ZOM 4, ZOM 8, ZOM 10, ZOM 13, B1_3, B2_3, B2_5, B3_2, B4_3, B4_6 and B5_2) to complement petrographic and geochemical data. Most of the minerals identified in XRD analysis were confirmed through SEM-EDX. Aluminosilicates, specifically muscovite (Fig. 13, spectrum Z2; Fig. 14, spectrum Z1), Fe (Fig. 13, spectrum Z1) and Ti oxides (Fig. 13, spectrum Z3; Fig. 15, spectrum Z2) were identified in the studied samples. Calcium phosphates were detected in samples B1_3, B2_3, B2_6 and B5_2 (Fig. 15, spectra Z1 and Z2). Pyrite was documented in samples B2_3, B2_6, B3_2, B4_3 (framboidal pyrite) and B4_6 (Fig. 14, spectrum Z3; Fig. 16, spectrum Z1), Cu sulfides in sample B2_3 (Fig. 14, spectrum Z2), arsenopyrite and chalcopyrite in sample B3_2 (also in B4_3 and B4_6 samples) associated with quartz (Fig. 16, spectra Z2 and Z4), probably related to hydrothermal fluids.

5.3. Reflectance of organic matter

In the absence of vitrinite in the studied samples dated from Silurian, reflectance measurements were carried out in vitrinite-like particles and graptolites. Table 2 resumes the results obtained for reflectance measurements, together with the number of measure particles and standard deviation. The mean random reflectance of vitrinite-like particles in samples collected near the Alandroal Cu occurrences varies between

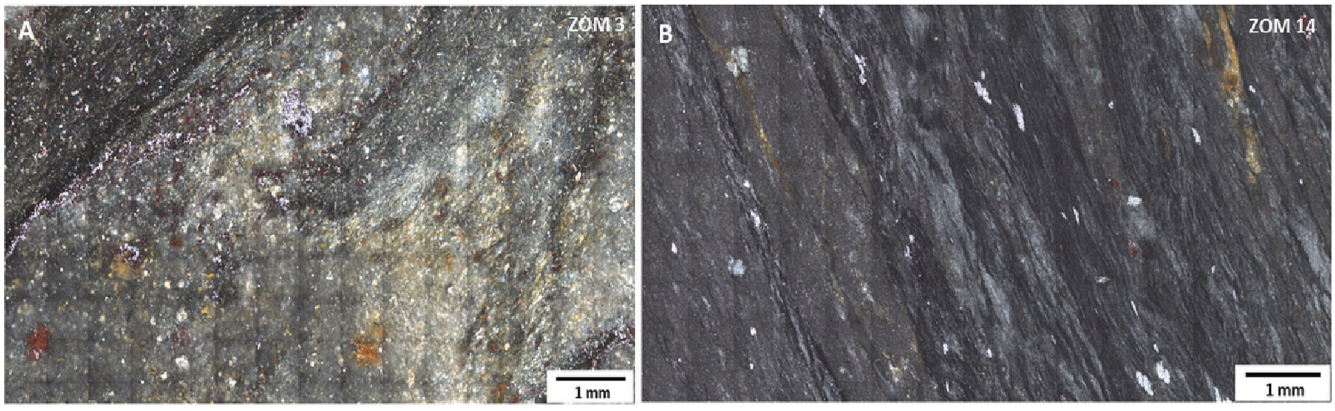

Fig. 8. Mosaics prepared from the assembly of photomicrographs taken from the polished blocks of rock pieces, exhibiting a general petrographic view and main features of samples ZOM 3 and ZOM 14.

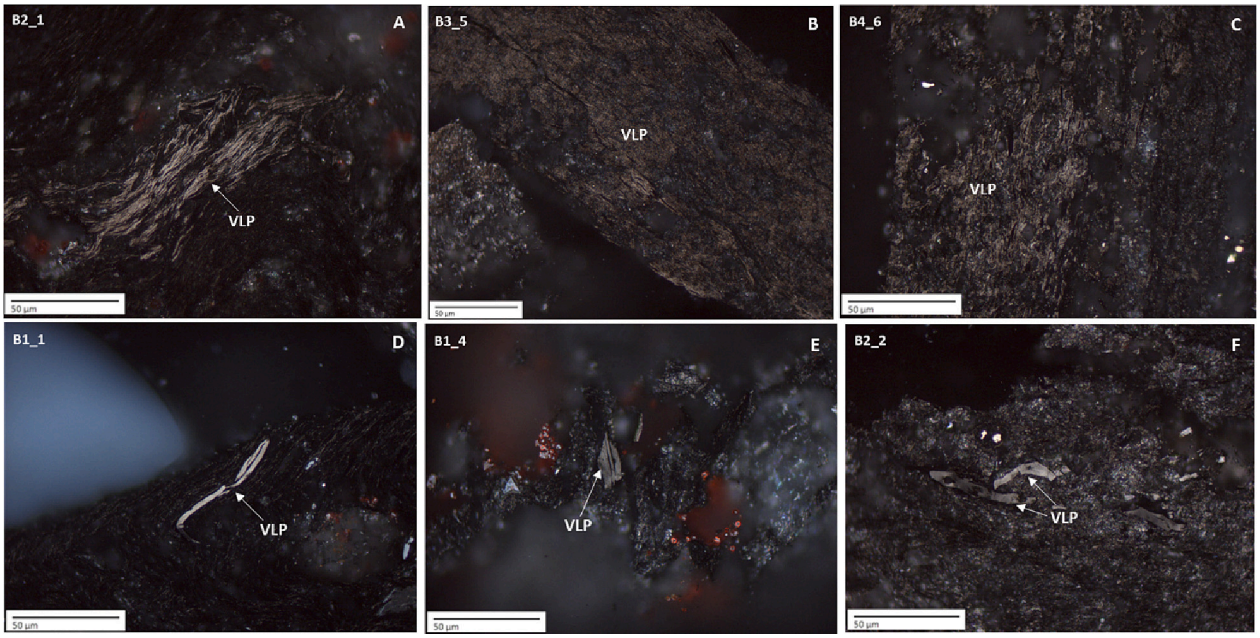

Fig. 9. A), B) and C) Photomicrographs showing the vitrinite-like particles (VLP), occurring interbedded along mineral matter; D), E) and F) Photomicrographs of vitrinite-like particles (VLP) exhibiting graphitic structures occurring as single flakes.

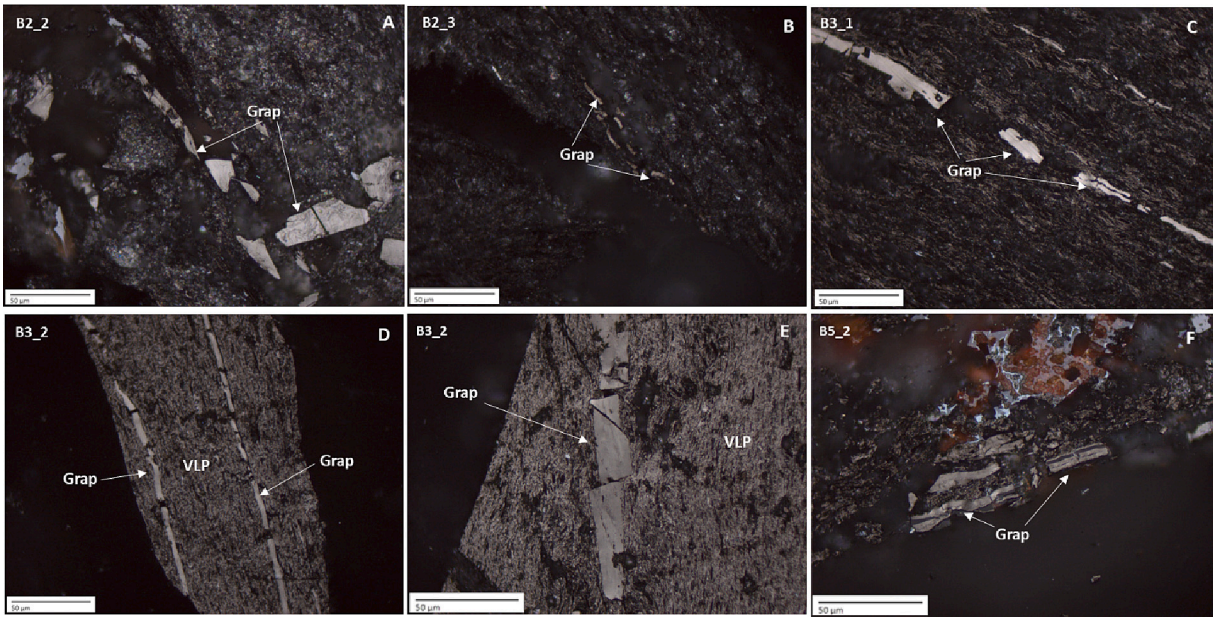

Fig. 10. A) to F) Photomicrographs showing graptolite fragments (Grap) interbedded with vitrinite-like particles (VLP) and mineral matter.

3.68% and 4.29%. Far from the mineralization, values of random reflectance of vitrinite-like particles range between 2.99% and 3.64% in Alandroal region, and between 1.93% and 5.36% in Barrancos (Table 2). As respect to the maximum reflectance, values near the Alandroal Cu occurrences varies between 6.48% and 7.67%, and far from Cu occurrences between 5.01% and 6.53% in Alandroal, and between 2.47% and 6.34% in Barrancos region (Table 2). The mean and maximum reflectance (Rr and R_{max}) in Miguel Vacas samples, measure in the vitrinite-like particles, ranges from 1.74% to 4.74% and from 2.27% to 6.66%, respectively.

In samples ZOM 10, ZOM 11, B2_2, B2_3, B3_1, B3_2 and B5_2, the reflectance was also measured in particles of graptolites (Rr_{grap}) since their occurrence is expressive in these samples and, on the other hand, few vitrinite-like particles were observed. The reflectance of zooclasts, such as graptolites, has been used to determine thermal maturity since reflectance data can be transformed to equivalent vitrinite reflectance values based on empirical correlations (e.g., Bertrand, 1990; Petersen et al., 2013; Hartkopf-Fröder et al., 2015). This means that graptolite reflectance may also be an indicator of thermal maturation of the host rocks (Suárez-Ruiz et al., 2012). The equivalent vitrinite reflectance for the studied samples was calculated ($VR_{r\text{-}eq}$ and $VR_{max\text{-}eq}$) according to Petersen et al. (2013) througth th equation: $VR_{eq} = 0.73 \times R_{grap} + 0.16$. The values of $VR_{r\text{-}eq}$ and $VR_{max\text{-}eq}$ range from 3.13% to 4.15% and from 4.86% to 5.31%, respectively in samples from Barrancos; and from 2.57% to 4.53% and from 4.06% to 6.53%, respectively in Miguel Vacas samples. Obtained values are concordant with mean and maximum

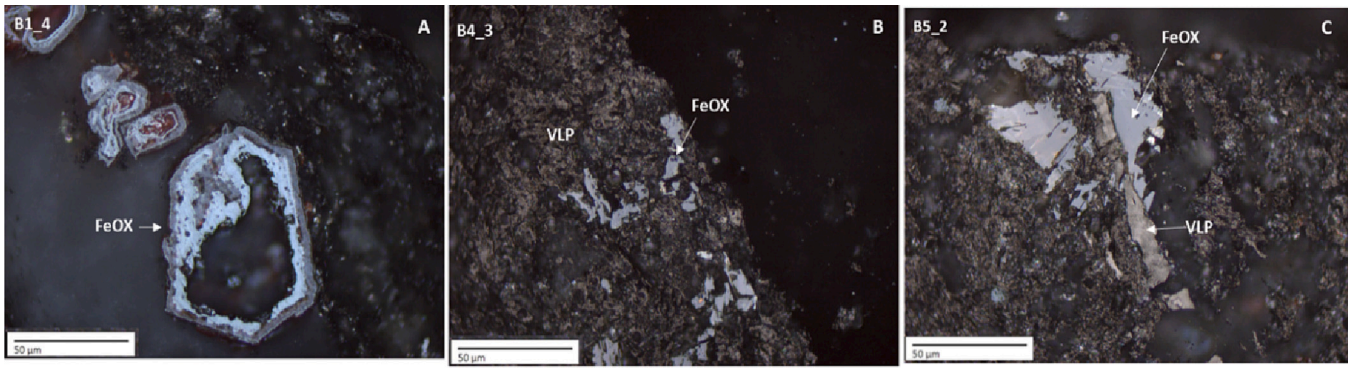

Fig. 11. A) to C) Photomicrographs of the presence of iron oxides (FeOX) interbedded with vitrinite-like particles (VLP).

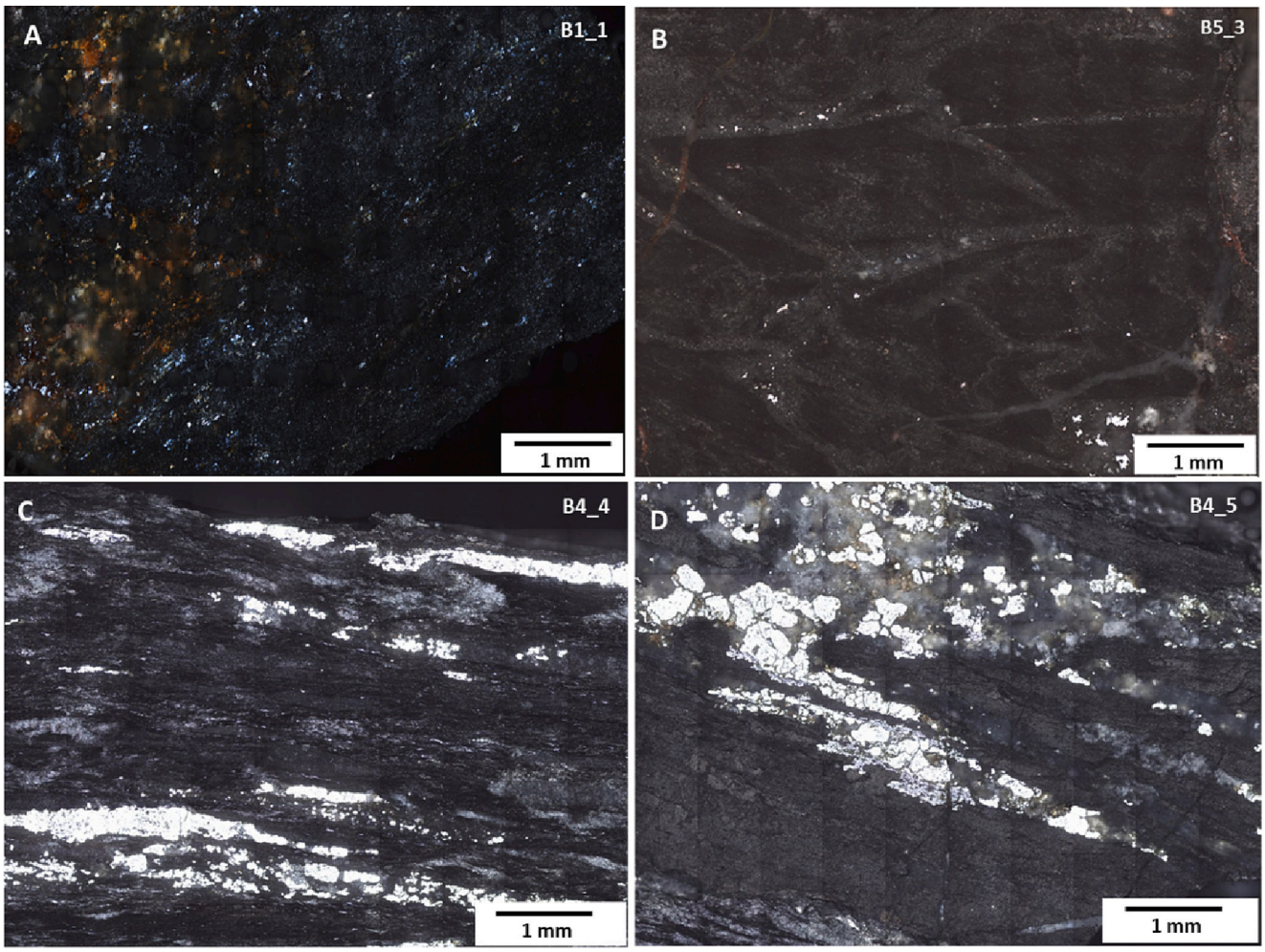

Fig. 12. Mosaics prepared from the assembly of photomicrographs taken from the polished blocks of rock pieces, exhibiting a general petrographic view and main features of samples B1_1, B5_3, B4_4, and B4_5.

reflectance values obtained in the other vitrinite-like particles.

5.4. Geochemical characterization of black shales

The TOC content and the concentration of major, minor and trace elements determined in the studied samples, together with the reference values for black shales (BBS) are presented in Table S2 and S3 (supplementary material).

The results reveal that TOC varies between 0.30% and 15.2% for Alandroal and Barrancos outcrop samples, and between 0.38% and 12.6% for Miguel Vacas samples (Table S2). Table 3 categorizes the analyzed samples according TOC values. Samples with higher TOC are those where the organic matter is noticeably more abundant under microscopic observations. Most of the samples have TOC values above 3%, samples from Alandroal area generally have low values of TOC, and samples from the drill cores B1 and B5 of Miguel Vacas present significantly lower TOC contents (Table 3).

From the analyzed major and minor elements, Al, Fe, and K are more abundant, followed by minor concentrations of Ca, Mg, Na, P and Ti. This geochemical composition pattern (Table S2) is consistent with the

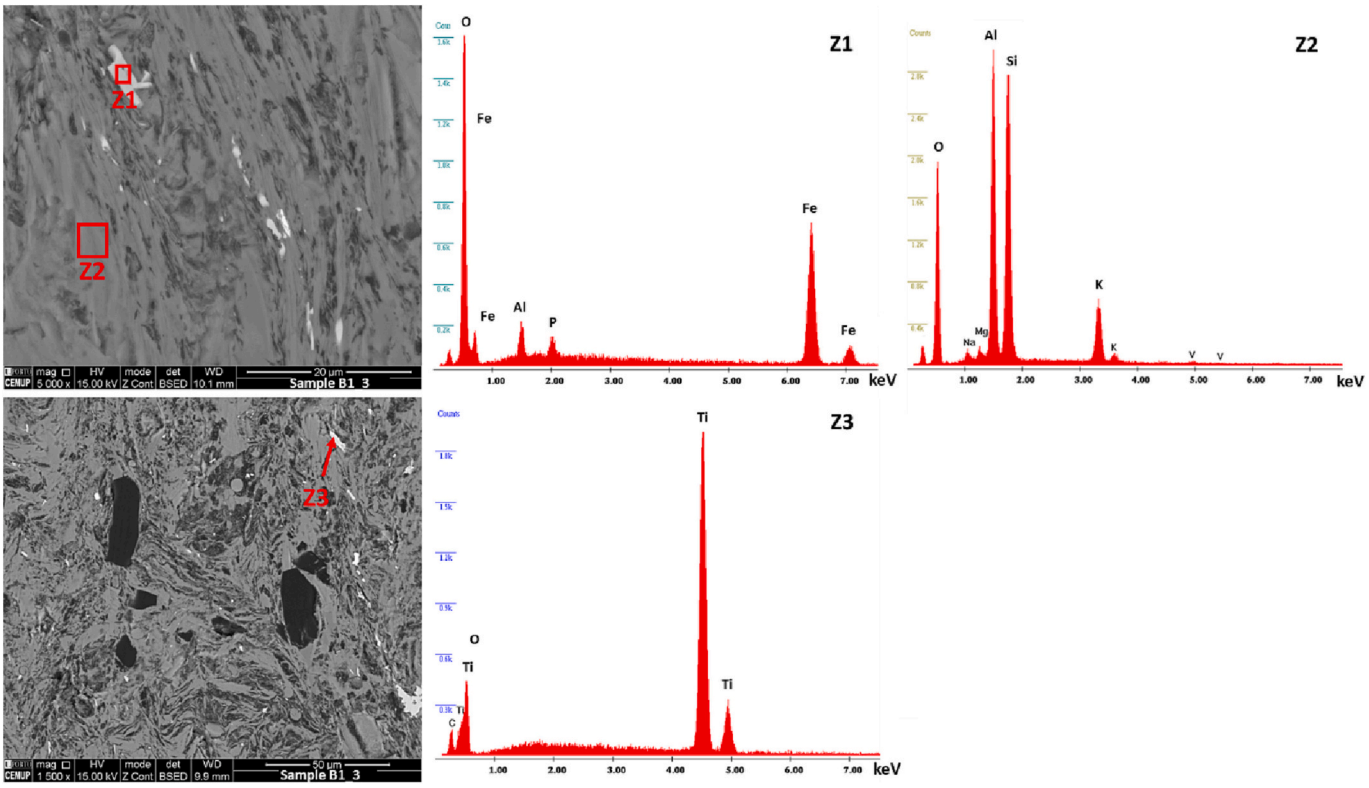

Fig. 13. SEM images and EDX spectra of iron oxides (Z1) and associated aluminosilicates (Z2) and titanium oxides (Z3) interbedded with aluminosilicates in sample B1_3.

mineralogical constituents identified through microscope observations including detrital minerals, mainly aluminosilicates, quartz, and iron oxides. Sulfur concentration is generally close to the detection limit. However, some samples have S concentration above 1%: B2_3, B2_5, B3_1, B3_2, B4_2, B4_3, B4_4, B4_5, B4_6 and B5_3 (Table S2).

Fig. 17 shows the concentration and the distribution pattern of trace elements. The elements with concentration consistently lower than <1 ppm are Cd, In, Re and Te, while Ag, Bi, Mo, Sb, Se, and Ta show concentrations above or below 1 ppm, depending on the group of samples (Fig. 17, Table S3). Relatively to the distribution pattern of the elements in samples from outcrops, some differences are noticed, standing out samples from Alandroal and Barrancos far from mineralization (Fig. 17B); the elements Ag, Pb, Mo, Sb, and Se generally have higher concentration in Barrancos samples (specifically in sample ZOM 10). These elements are known to have affinity with organic matter (Finkelman et al., 2018). Otherwise, the sample ZOM 13 reveals lower concentrations of Ag, Cd, Pb, Te and U. Samples from Alandroal region, near to the mineralization (Fig. 17A), reveal higher concentrations of Cu and Mn, being only compared with some values in samples from Miguel Vacas drill cores.

Considering the mean chemical composition of samples from each drill core from Miguel Vacas, it is possible to observe that they have generally a similar pattern (Fig. 17C). However, some differences are noticed and the most relevant are: B3 presents higher concentrations of Ag, As, Cu, Sr and V; B1 shows lower concentrations of Ag, Cd, Mo and Pb (Fig. 17C, Table S2).

It is also possible to observe that, in general, the samples from Barrancos and Miguel Vacas with the most depleted profile in REE (Figs. S1 and S2) have in common the fact that are the samples with lower Cu values when compared to the others. In Barrancos, the sample ZOM 10 (Fig. S1B) present a depleted profile and low Cu concentration (32.0 ppm) when compared to the ZOM 11. Samples B1_2, B2_5, B4_4, and B5_1 from Miguel Vacas have Cu concentrations around 30 ppm and have, generally, the most depleted profiles (Fig. S2).

The concentration of rare earth elements (REE) in the studied samples is presented in Table S3. The ΣREE varies from 115 ppm to 663 ppm, with an average value of 244 ppm for the outcrop samples, and from 27.5 ppm to 702 ppm, with an average value of 218 ppm for Miguel Vacas samples (Table S3). The samples from outcrops show consistently higher concentrations of light REE (LREE >100 ppm) and heavy REE (HREE ≥10 ppm) compared to drill core samples.

The REE profiles of the black shale samples normalized to BBS (maximum value; Ketris and Yudovich, 2009), presented in the supplementary material (Figs. S1 and S2), are relatively similar, showing lightly flattened profiles. Samples from B3 (Fig. S2C) evidence more differentiated and enriched profiles when compared with the other group of samples, while samples B1_2, B1_5 and B2_5 have a very depleted profile (Fig. S2A and S2B).

All samples have a positive anomaly of Pr and Eu (except sample ZOM 9 and ZOM 14 for Eu). In contrast, the REE profiles show slight negative anomaly of Ce, Nd and Tm. The positive Eu anomaly can be associated with the presence of detrital or hydrothermal plagioclase (Boyong et al., 2011), which is consistent with the XRD analysis.

6. Discussion

6.1. Maturation and paleotemperature

The maturation of dispersed organic matter in rocks is a process that affects the organic matter after its deposition, resulting from the burial history and being controlled by an increase and duration of heating and pressure (Suárez-Ruiz et al., 2012). To evalute the maturation of the organic matter, the classification proposed by Kwiecinska and Petersen (2004) based on the R_{max} values was considered. The organic matter in the studied samples can be classified between the rank stage of anthracite, when 2.0% < R_{max} < 5.0%, and meta-anthracite, when R_{max} ranges from 5.0% to 6.5%. Anthracite and meta-anthracite are natural precursors of semi-graphite when organic matter is subjected to high

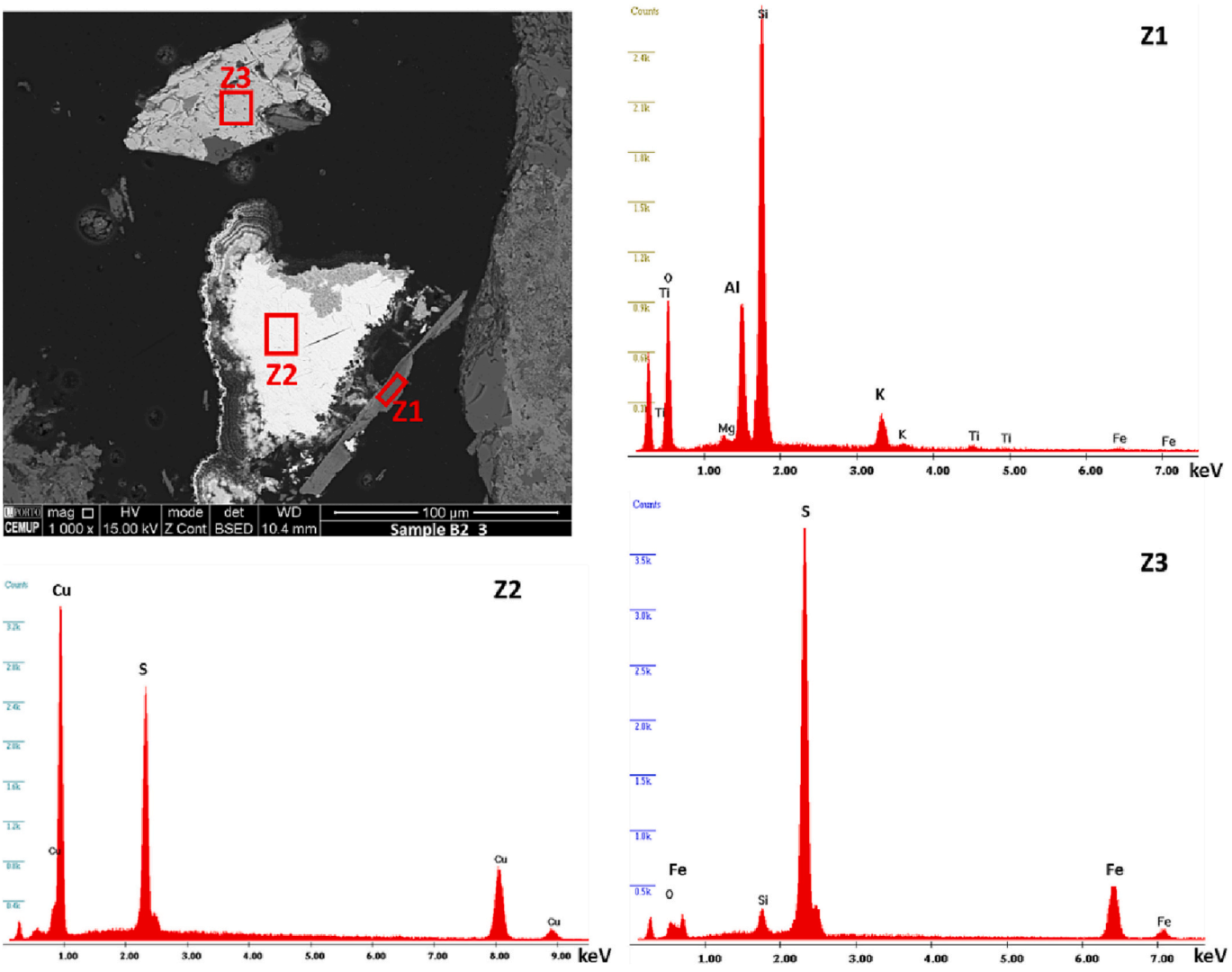

Fig. 14. SEM image and EDX spectra of aluminosilicates (Z1), copper sulfide (Z2) with zonation at the edges of the particle, and iron sulfide (Z3) in sample B2_3.

geothermal gradient, and/or to high pressure and/or tectonic stress. Anthracite, meta-anthracite, and semi-graphite are transitional phases of graphite that represent varying degrees of graphitization of carbon contained in the organic matter with growing molecular structure order (Li et al., 2022).

Fig. 18 presents the determined mean and maximum reflectance values, as well as the fields for anthracite, meta-anthracite, and semi-graphite classification. Samples from Alandroal area (near the mineralization), with the exception of ZOM 9, correspond to semi-graphite stage with $R_{max} > 6.5\%$ (Fig. 18A). The organic matter in samples far from the mineralization (including from Alandroal and Barrancos) have a maturation range between meta-anthracite (ZOM 13, ZOM 11 and ZOM 10) and semi-graphite (ZOM 14) (Fig. 18A). Generaly, samples near mineralization present higher organic matter maturation, possiby resulting from thermal maturation associated to hyrothermal fluids.

As respect to the samples from the drill cores (Figs. 18B to 18F), the maturation of organic matter varies between the range of anthracite and semigraphite, although most of samples show a thermal maturation compatible with the anthracite rank. Only samples B3_2 and B5_5 have R_{max} higher than 6.5%, thus in the semi-graphite field (Fig. 18D and F), and therefore higher maturation. Samples from B2, B3, and B5 do not exhibit variable maturation of organic matter with depth, presenting a hererogenous pattern, while in drill cores B1 and B4, the maturation seems to show an increase trend with depth (Figs. 18 and 19).

The reflectance of organic matter can also be used to estimate paleotemperatures associated with the maturation and discuss the processes that condition it, as for example, tectono-metamorphic activity, circulation of hydrothermal fluids or magmatic intrusions (e.g., Eakin and Gize, 1992; Landais, 1993). The estimation of paleotemperatures based on reflectance of organic matter can be made using Barker and Pawlewicz (1994) equation: $T_{max} = (\ln Rr + 1.19)/0.00782$, being Rr the vitrinite random reflectance. This equation considers that the hydrothermal metamorphism includes hydrothermal ore deposits and active geothermal systems.

The maximum temperatures estimated for the studied samples are presented in Table 2, and were calculated considering the random reflectance of vitrinite-like particles for the majority of samples and the random equivalent vitrinite reflectance in samples ZOM 10, ZOM 11, B2_2, B2_3, B3_1, B3_2 and B5_2.

Generally, outcrop samples show higher values of paleotemperatures (> 300 °C) than the drill core samples from Miguel Vacas. The paleotemperatures vary between 319 °C and 338 °C in Alandroal area near the mineralizations, between 292 °C and 317 °C in Alandroal area far from mineralization, and between 298 °C and 334 °C in Barrancos area (Table 2). In Miguel Vacas samples the value of paleotemperatures range from 223 °C to 351 °C (Table 2).

The irregular profiles of maturation with depth in the Miguel Vacas drill cores, often with lower mean random reflectance values (Rr)

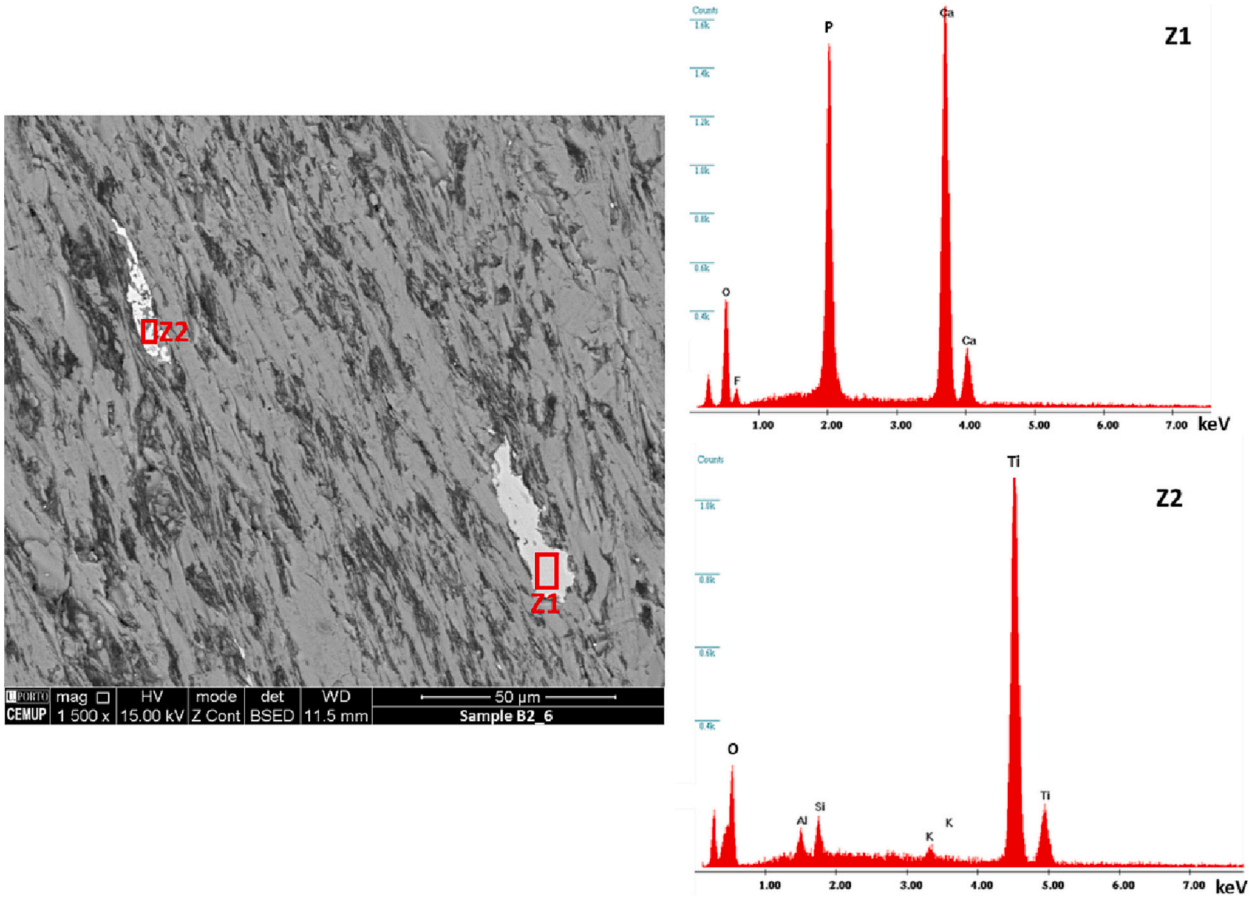

Fig. 15. SEM image and EDX spectra of calcium phosphate (Z1), titanium oxide (Z2), and organic matter within aluminosilicates in sample B2_6.

underlying higher values of reflectance of organic matter (Fig. 19), could be related to the circulation of hydrothermal fluids. Indeed, some authors (e.g., Barker, 1991; Glikson and Mastalerz, 2000) concluded that these irregular profiles are a characteristic feature of organic matter that matured through fast heating due to irregular heat distribution in hydrothermal-geothermal systems. The higher values of mean random reflectance were detected at variable depths, an even at different levels within drill cores B2, B3, and B5, displaying a vertical and lateral variation on the reflectance of organic matter. This supports that the maturation resulted from the circulation of hydrothermal fluids related with Cu-ore deposit genesis. The localized higher values of paleotemperatures in some samples may indicate the proximity to the mineralized vein or local veining (Table 2; Fig. 19).

The higher values of reflectance of the outcrop samples ZOM 2, ZOM 3 and ZOM 4 could be explained by the proximity to Mociços Cu vein deposit (Fig. 2A). However, sample ZOM 1, located 1 km to SW (Fig. 2A) show similar values of refletance, which can indicate a more regional pattern of fluid circulation. Nevertheless, the discrepant maturation associated with hydrothermal evolution of Cu-ore deposits do not explain all the pattern, and a regional model should be considered (see section 5.5).

6.2. Elements enrichment and mode of occurrence

The concentration coefficients (CC) were calculated in order to compare the geochemical composition of samples with standard values, namely the BBS (Ketris and Yudovich, 2009). The CC were calculated through the ratio between elements concentration in the studied samples and their concentration in reference data, and provides information about the depletion (CC $<$ 1) or enrichment (CC $>$ 1) of elements comparatively with BBS. The CC were determined considering the maximum reported values for BBS. The CC of REE were estimated considering the sum of LREE and HREE. Table 4 shows the group of elements classified according with Dai et al. (2015, 2016): significant enriched CC $>$ 10; slightly enriched 2 $<$ CC $<$ 10, normal 1 $<$ CC $<$ 2; and depleted CC $<$ 0.5.

Most elements are depleted or have concentrations close to the values reported for BBS, this is, concentrations identified as normal (CC $<$ 1) to slightly enriched (1 $<$ CC $<$ 2) (Table 4), both in the outcrop samples and in the drill core samples.

As respect to the outcrop samples, the majority of the samples shows normal to slightly enriched concentrations of most elements. Exception to Barrancos samples, which are slightly enriched in Sb and Ag, mainly in sample ZOM 11 (Table 4). In Alandroal region, it should be highlighted the enrichment of Cu (2 $<$ CC $<$ 10) in two samples collected near the Mociços Cu deposit (ZOM 3 and ZOM 4). The presence of Cu secondary phases (malachite) as trace mineral in ZOM 3 was identified XRD studies, which can explain the enrichment in Cu in those samples. Other elements as Th, Rb, V, REE, Li, Be, and Cs are occasionally enriched in some outcrop samples (2 $<$ CC $<$ 10).

As respect to Miguel Vacas drill cores, the enrichment of Ag, As, Cu, V, and REE is noticeable in several samples, namely in black shales from B3, featuring CC $>$ 10 for Ag and V (Table 4). The drill core B3 shows significant enrichment in Cu in all samples with exception to the most superficial one. It should be emphasized that this is a transversal behavior in the most superficial studied sample of all drill cores. The elements Cr, Ni, Th, Mo, Mn, and Sn are also occasionally enriched in some drill core samples (2 $<$ CC $<$ 10).

To understand the elements mode of occurrence of Alandroal (near mineralization) and Miguel Vacas samples, the Pearson correlation

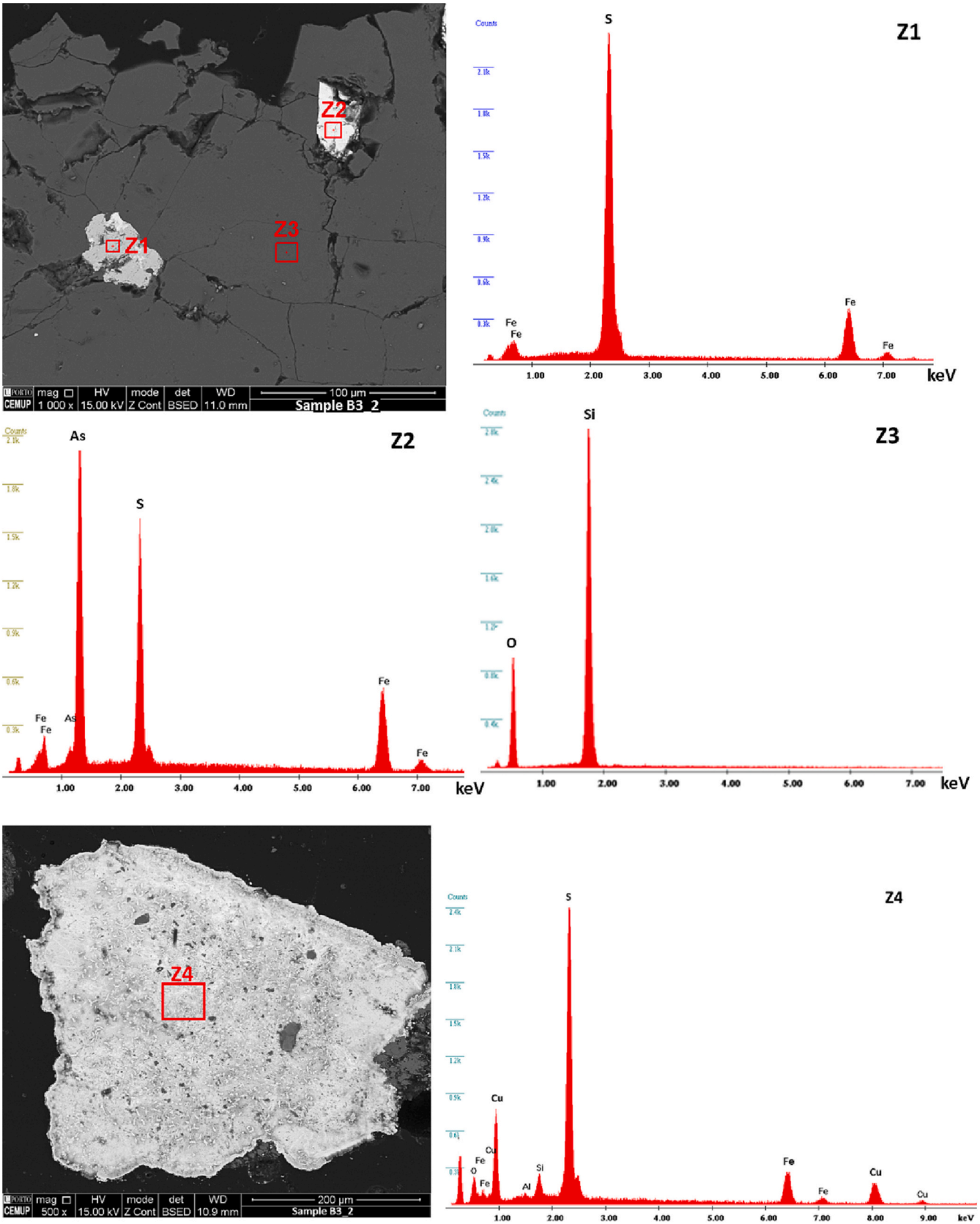

Fig. 16. SEM images and EDX spectra of pyrite (Z1), arsenopyrite (Z2), quartz (Z3), and chalcopyrite (Z4) in sample B3_2.

Table 2
- Mean (Rr) and maximum reflectance (R_{max}) measured in vitrinite like-particles, equivalent vitrinite mean ($VR_{r\text{-}eq}$) and maximum reflectance ($VR_{max\text{-}eq}$) estimated based on graptolites reflectance, and estimated paleotemperatures based on the random mean reflectance of the studied samples.

		Sample	Depth (m)	Measurements in vitrinite like-particles					Measurements in graptolites					
				N	Rr (%)	SD	R_{max} (%)	SD	N (grap)	$VR_{r\text{-}eq}$ [1]	SD (grap)	$VR_{max\text{-}eq}$ [1]	SD (grap)	Paleotemperature [2] (°C)
Alandroal	**Near mineralization**	ZOM 1	–	35	3.92	0.74	6.97	1.51	–	–	–	–	–	327
		ZOM 2	–	47	4.29	1.13	7.08	1.40	–	–	–	–	–	338
		ZOM 3	–	32	4.03	0.62	7.25	1.16	–	–	–	–	–	330
		ZOM 4	–	36	4.09	0.58	7.67	1.24	–	–	–	–	–	332
		ZOM 8	–	32	3.90	0.84	7.12	1.87	–	–	–	–	–	326
		ZOM 9	–	20	3.68	0.80	6.48	1.32	–	–	–	–	–	319
	Far from mineralization	ZOM 13	–	24	2.99	0.74	5.01	1.35	–	–	–	–	–	292
		ZOM 14	–	5	3.64	1.13	6.53	2.76	–	–	–	–	–	317
Barrancos		ZOM 10	–	12	5.36	0.40	6.34	0.59	52	4.15	0.59	5.31	0.86	334*
		ZOM 11	–	11	1.79	0.42	2.47	0.89	12	3.13	1.36	4.86	1.87	298*
Miguel Vacas	**B1**	1	25.4	10	2.68	1.18	3.90	2.12	–	–	–	–	–	278
		2+	42.7	8	3.29	0.97	5.67	2.02	–	–	–	–	–	304
		3+	52.1	19	3.55	0.68	4.44	0.88	–	–	–	–	–	314
		4+	55.5	11	3.34	0.74	5.14	1.14	–	–	–	–	–	306
		5	84.0	16	3.31	0.70	5.76	1.35	–	–	–	–	–	305
	B2	1	37.0	21	2.84	0.62	5.08	1.33	–	–	–	–	–	286
		2	46.7	3	4.21	0.49	5.97	0.73	37	4.06	1.64	6.22	1.33	331*
		3	49.9	7	2.91	0.88	4.72	1.07	19	2.57	0.74	4.06	0.93	273*
		4	64.1	15	2.34	0.58	3.20	0.98	–	–	–	–	–	261
		5+	97.1	15	3.09	0.64	3.49	0.84	–	–	–	–	–	296
		6+	127.9	11	1.78	0.49	2.57	0.83	–	–	–	–	–	226
	B3	1	12.4	19	3.21	0.71	4.74	1.17	27	4.16	2.18	5.74	1.73	334*
		2	29.5	14	4.27	0.94	5.34	1.58	27	4.53	1.69	6.53	1.71	345*
		3	55.0	13	3.96	0.99	5.46	1.75	–	–	–	–	–	328
		4+	81.5	15	4.14	1.22	5.42	1.33	–	–	–	–	–	334
		5+	96.6	21	2.75	1.23	3.74	1.06	–	–	–	–	–	282
	B4	1	24.4	14	1.74	0.42	2.43	0.95	–	–	–	–	–	223
		2	43.7	12	2.78	0.46	4.10	1.04	–	–	–	–	–	283
		3	70.4	32	3.80	0.85	4.53	1.08	–	–	–	–	–	323
		4+	130.6	18	2.25	0.57	4.06	1.00	–	–	–	–	–	256
		5+	144.9	10	2.74	0.47	3.79	0.88	–	–	–	–	–	281
		6+	169.7	17	3.30	0.80	4.63	1.14	–	–	–	–	–	305
	B5	1	22.3	4	4.63	0.59	5.92	1.17	–	–	–	–	–	348
		2+	36.3	14	2.85	0.69	4.18	0.73	36	2.96	1.17	4.48	1.28	291*
		3	50.2	18	2.86	0.97	3.67	1.04	–	–	–	–	–	287
		4+	105.0	5	4.74	1.47	5.43	1.67	–	–	–	–	–	351
		5+	119.2	10	2.92	0.73	4.53	1.00	–	–	–	–	–	321
		6+	137.6	9	3.73	0.73	6.66	1.00	–	–	–	–	–	243
		7+	139.9	2	2.04	0.24	2.27	1.16	–	–	–	–	–	289

+ samples proximal to mineralized veins; N - number of measured vitrinite like-particles; N_{grap} - number of measured graptolites particles; SD - standard deviation; [1] $VR_{eq} = 0.73 \times R_{grap} + 0.16$ (Petersen et al., 2013); [2] $T_{max} = (\ln Rr + 1.19)/0.00782$ (Barker and Pawlewicz, 1994); * values calculated from equivalent vitrinite reflectance of graptolites.

Table 3
Total organic carbon of the studied samples.

TOC	Samples
> 10%	ZOM 10 B2_3, B3_1, B4_3, B4_6
10% - 8%	B1_3, B2_4, B3_2, B3_5, B4_1, B4_2
8% - 3%	B1_5, B2_1, B2_2, B4_4, B4_5
3% - 1%	ZOM 11, ZOM 14 B1_1, B1_4, B2_5, B2_6, B3_3, B5_1, B5_2, B5_6, B5_7
< 1%	ZOM 1, ZOM 2, ZOM 3, ZOM 4, ZOM 8, ZOM 9, ZOM 13 B1_2, B3_4, B5_3, B5_4, B5_5

coefficients were calculated, and particular consideration was given to enriched elements ($2 < CC < 10$). The samples from Alandroal far from mineralization and Barrancos were not included since they present discrepant values in comparison with the remaining outcrop samples. Table 5 shows the Pearson correlation coefficients for selected elements and positive correlations significant at $p < 0.05$ are identified in blue at, while negative correlations significant at $p < 0.05$ are marked in red.

The results reveal a significant positive correlation coefficient between TOC and S, Cr and U ($r \geq 0.65$, $p < 0.05$; Table 5) and a positive association with Mo, Ni, Pb, Sb and V ($r > 0.40$, $p < 0.05$; Table 5), which is an organic elemental association generally reported in several studies (Swaine, 1990; Liu et al., 2015; Finkelman et al., 2018; Laranjeira et al., 2023a).

The positive correlation between TOC and S ($r = 0.65$, $p < 0.05$; Table 5) indicates the occurrence of sulfides in association with organic matter, which corroborates the petrographic and SEM-EDX analysis. The strong positive correlation between S and Ni ($r = 0.83$, $p < 0.05$; Table 5), between S and Pb ($r = 0.68$, $p < 0.05$), and weak positive association with other metals such as Fe, Co, Cr, Cu, Pb and Sb indicate that S is partially inorganically bound.

Other elements have a negative correlation with TOC and a positive correlation with Al, pointing out their association with aluminosilicates (El-Anwar et al., 2018; Finkelman et al., 2018; Laranjeira et al., 2023a). These include the elements Ti ($r = 0.86$, $p < 0.05$), Cs ($r = 0.78$, $p < 0.05$), Nb ($r = 0.84$, $p < 0.05$), Sc ($r = 0.91$, $p < 0.05$), and Th ($r = 0.72$, $p < 0.05$).

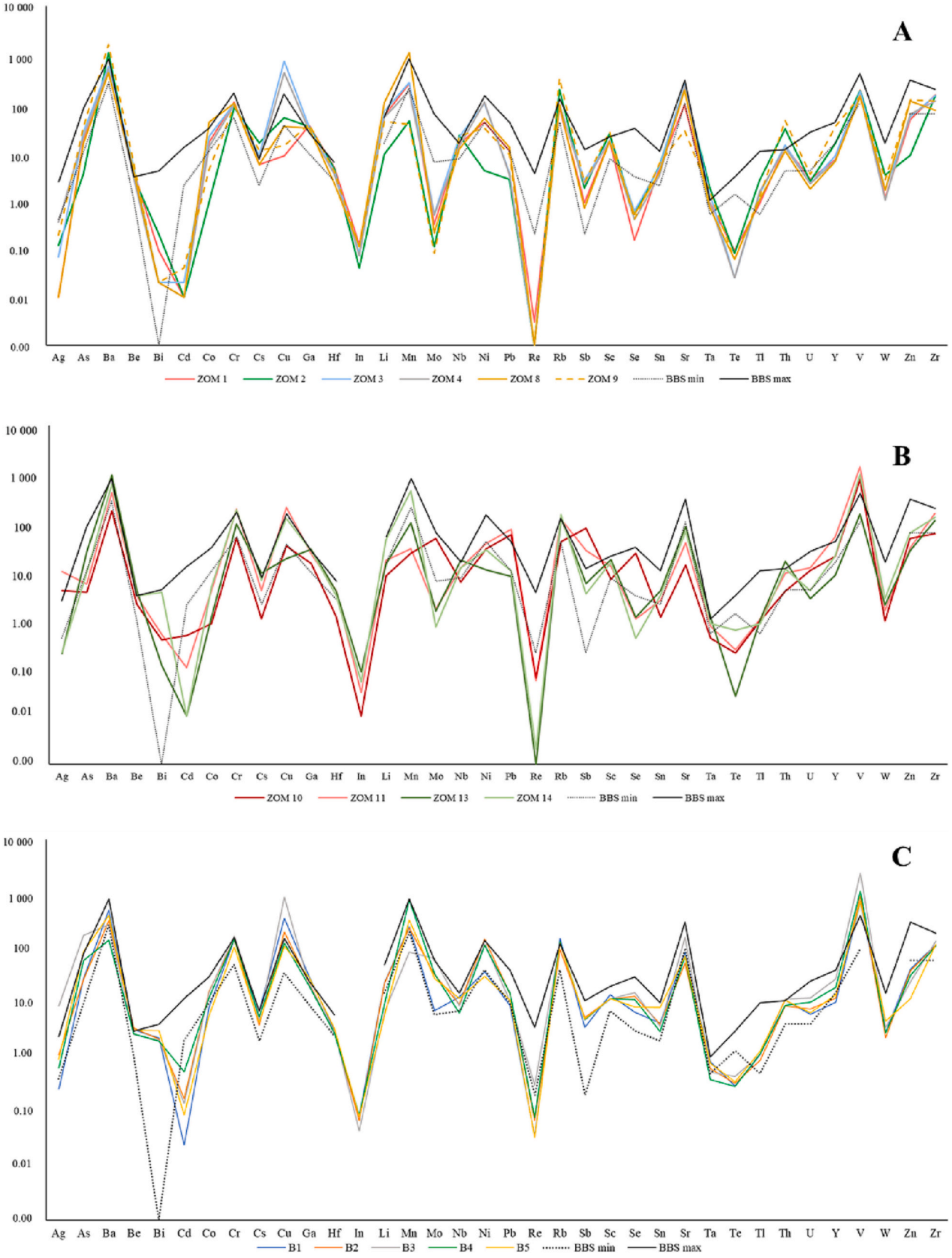

Fig. 17. Concentration of trace elements (ppm) in samples from: A) Alandroal area near to the mineralizations; B) Alandroal and Barrancos area far from mineralization; C) Miguel Vacas area (each line represents the mean chemical composition of samples from each drill core). Range of BBS is also represented.

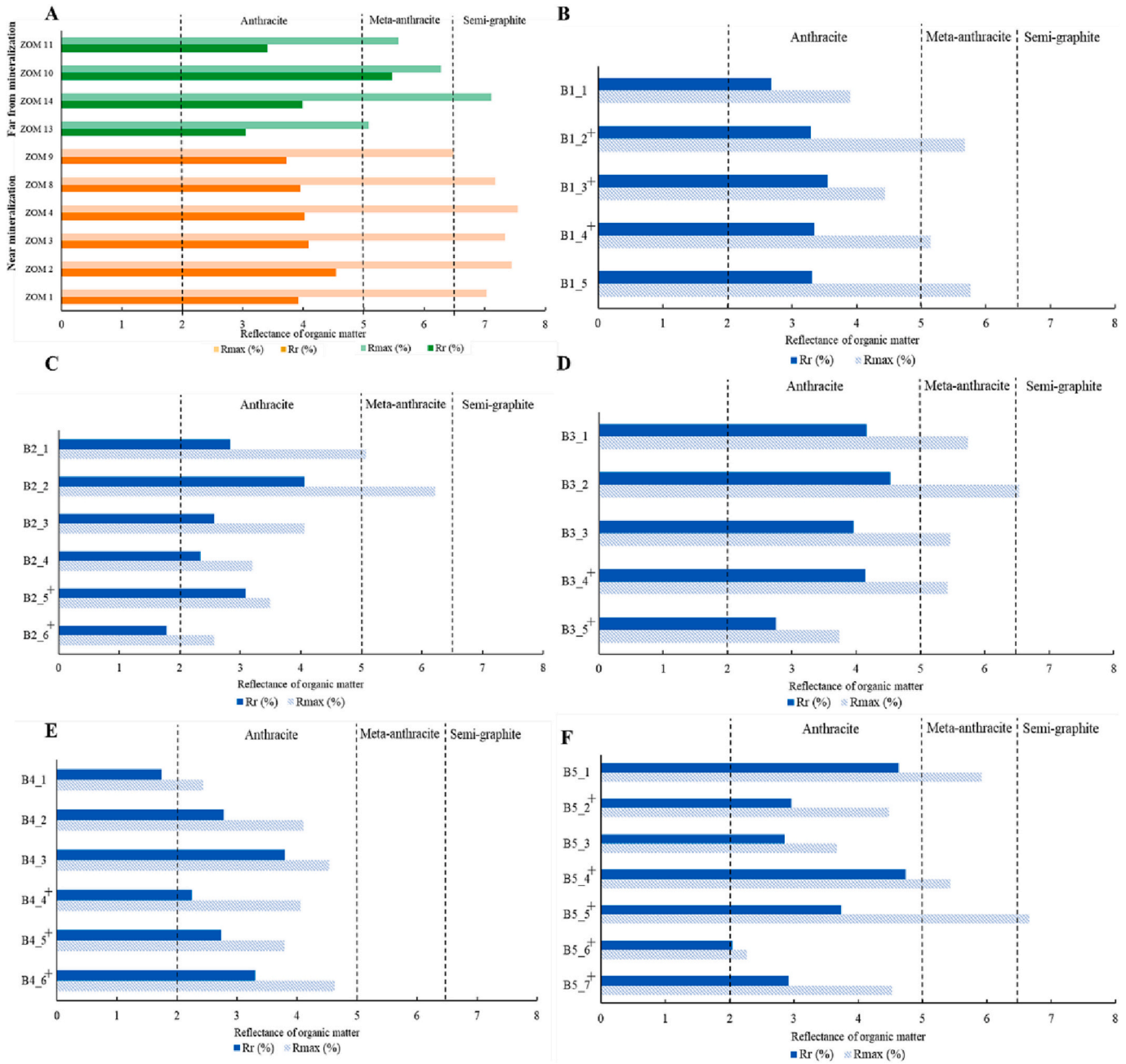

Fig. 18. Mean and maximum reflectance of organic matter in: A) samples near and far from the mineralizations, from Alandroal and Barrancos area; B) samples from B1; C) samples from B2; D) samples from B3; E) samples from B4; F) samples from B5.

6.3. *Redox sensitive elements and paleo-redox conditions*

Paleodepositional environments include oxic, suboxic or anoxic conditions. Anoxic conditions may be non-sulfidic or sulfidic; in the latter case, they are also designated euxinic when H_2S occurs within the water column. Suboxic environments are characterized by extremely low but generally nonzero O_2 concentrations in the water column, where H_2S is limited to pore waters below the sediment-water interface. Under oxic conditions, aerobic organisms can use dissolved O_2 from the overlying and interstitial waters for their metabolism. As dissolved O_2 becomes depleted, the organic matter decomposition continues via organisms using secondary oxidant sources: nitrate, manganese oxides and iron oxides, oxyhydroxides, and sulfate (Tribovillard et al., 2006).

Some trace elements, such as Cd, Co, Cr, Mo, Ni, Th, U, and V, are sensitive to variations of oxygenation conditions during deposition. Some ratios (e.g., Ni/Co, V/Cr and Th/U) have been widely used as an indicator for understanding the paleo-redox conditions during deposition processes (e.g., Hatch and Leventhal, 1992; Jones and Manning, 1994; Rimmer, 2004; Tribovillard et al., 2006; Ross and Bustin, 2009). These ratios should be used with some caution and critically when studying material that may be affected by weathering due to the sensitivity of some of these elements.

The ratios Ni/Co, V/Cr and Th/U were calculated for the studied samples (Table 6). Higher values of the ratio Ni/Co are related to progressively lacking O_2 during the deposition of the sediments (Jones and Manning, 1994), due to the relative facility of Ni to concentrate in sediments deposited under reducing conditions (e.g., Shaw et al., 1990; Emerson and Huested, 1991; Jones and Manning, 1994). In turn, Co concentration is considered to depend on detrital content, and not influenced by redox conditions (Dill, 1986; Ross and Bustin, 2006).

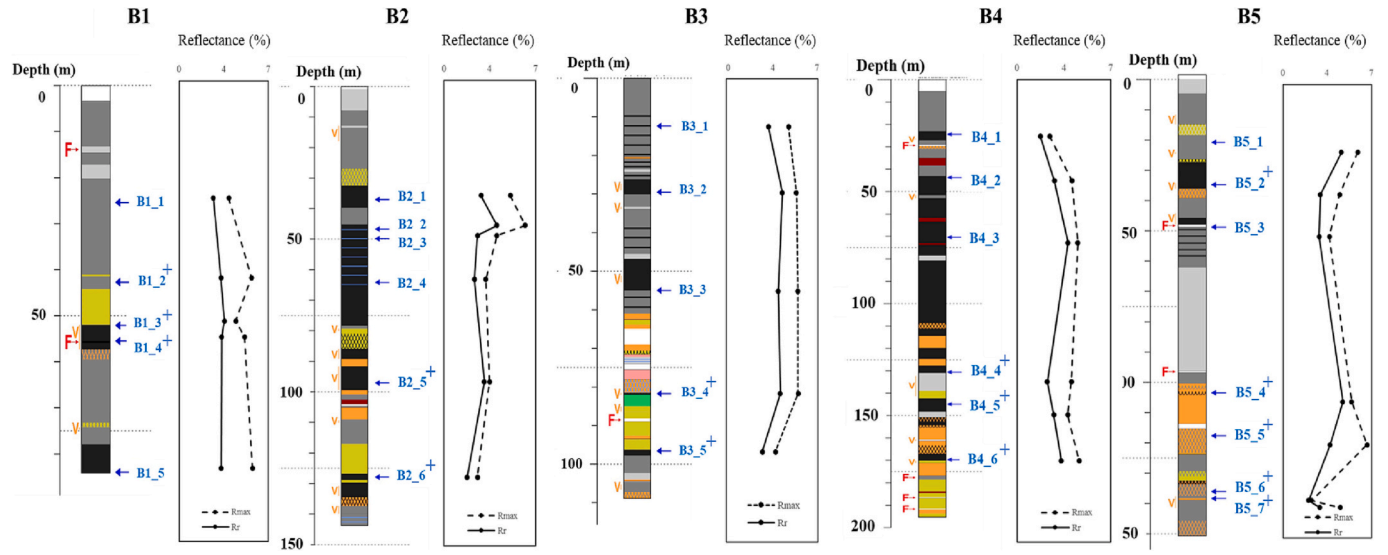

Fig. 19. Maturation profiles in Miguel Vacas.

Therefore, higher values of Ni/Co ratio (> 7) indicate anoxic conditions, while lower values (< 5) indicates oxic conditions (e.g., Galarraga et al., 2008; Pi et al., 2014; Eric et al., 2019). Other authors also suggested that V is more concentrated in sediments deposited under reducing conditions (e.g., Shaw et al., 1990; Emerson and Huested, 1991; Jones and Manning, 1994), being considered that V/Cr ratio above 2 indicate anoxic depositional conditions, while values below 2 are indicative of an oxic environment (Jones and Manning, 1994).

The higher Ni/Co and V/Cr are found in samples ZOM 10, ZOM 11, B1_3, B1_4, all samples from B2 (with exception of B2_1), B3_1, B3_2, all samples from B4 (except B4_4 and B4_5), B5_1 and B5_2, which suggest more anoxic conditions during deposition (Fig. 20). These samples, generally, are those with higher TOC values.

Considering the Th/U ratio, Th is relatively immobile in the low-temperature surface environment, being concentrated during weathering in resistant minerals and is usually found in the detrital fraction associated with heavy minerals or clays (Jones and Manning, 1994). On the other hand, U may be fixed under reducing conditions (Jones and Manning, 1994). Consequently, values of Th/U < 2 represent anoxic conditions. According to this ratio, both samples from Barrancos (ZOM 10 and ZOM 11) and the majority of samples from Miguel Vacas drill cores seems to be deposited in anoxic conditions (Table 6), with exception of eight samples (B1_1, B1_2, B1_5, B4_4, B5_4 to B5_7).

The ratios Ni/Co, V/Cr, and Th/U (Table 6) reveal that, generally, samples from Alandroal (far from mineralization) and Barrancos seems to be deposited in an anoxic depositional environment, while samples from Alandroal (near mineralization) have ratios that indicate their formation under oxic to suboxic conditions. The samples from Miguel Vacas do not have a consistent behavior, although the paleo-redox ratios indicate that most of samples have been deposited in suboxic to anoxic conditions. Similar paleo-redox conditions were also described to the Silurian succession from OMZ (Piçarra, 2000; Robardet and Gutiérrez-Marco, 2004; Roseiro et al., 2020), and also in several places around the world (e.g., Semtner and Klitzsch, 1994; Melchin et al., 2012).

6.4. Organic matter and mineralization processes: What connection?

Organic matter can have a significant influence on the behavior of mineralizing systems (Greenwood et al., 2013). Previous studies provided evidence of a strong association between occurring minerals and organic matter (Greenwood et al., 2013) and, therefore, it is important the analysis of the variations of the elements and the TOC in the studied samples.

Fig. 21 presents the concentration of selected elements to compare the general pattern between the regional background (Alandroal and Barrancos far from mineralization) with the samples near the mineralization in Alandroal region (including Miguel Vacas). In general, although similar concentrations are denoted, data show some particularities:

- the Ag and Cr median values of outcrop samples from Alandroal and Barrancos, far from mineralization, are generally higher when compared to the remaining samples, although maximum values were obtained in Miguel Vacas drill cores;
- median Cu concentrations are generally similar in all sample domains, but maximum values in Alandroal near mineralization and Miguel Vacas are around 10× superior as respect to the background, and minimum values are inferior to the minimum of background;
- the As content in Miguel Vacas is significantly higher when compared with other domains;
- the Co and Ni contents show similar behavior, with a significant increase of content in Alandroal near mineralization and Miguel Vacas; similar behavior is also identified in Fe content.

Pearson correlation coefficients allow to discuss some of the previous mentioned relations. The variation of Co and Ni concentrations indicates a positive correlation between these elements ($r = 0.73$, $p < 0.05$; Table 5). The high coefficients between both elements and P, S and Fe ($r > 0.5$, $p < 0.05$; Table 5) seems to indicate a possible association between phosphate phases and pyrite (which incorporate Co and Ni), possibly associated with organic-rich sedimentation of black shales. Although the coefficients between Ni, S and P, and TOC is significant ($r > 0.5$, $p < 0.05$; Table 5), similar behavior is not registered for Co ($r \approx 0.1$). The positive correlation between As and Ag contents in black shales ($r = 0.70$, $p < 0.05$; Table 5) seems to indicate their association to the same mineral phase. The increase of both elements should be related with the presence of dispersed sulfides (arsenopyrite and arsenic pyrite) in Miguel Vacas black shales related with ore deposit (Fig. 12C and D; Fig. 16). It should be emphasized that those phases are also identified in black shales from other areas, being associated with organic matter.

In Figs. 22 and 23 are presented the elemental variation profiles along the drill core samples from Miguel Vacas, with the representation of TOC, S, paleotemperatures, Fe, As, Cu, V, and the paleoredox ratios Th/U and Ni/Co. The TOC content display vertical variations along the drill cores. Generally, the TOC peak is coincident with the peak of V, showing their association (also indicated by high values of CC; Table 4).

Table 4
Concentration coefficients (CC > 1) of trace elements in the studied samples relatively to BBS.

	Samples	1 < CC < 2	2 < CC < 10	CC > 10
Alandroal near mineralization	ZOM 1	Be, Ga, Li, Th, LREE	–	–
	ZOM 2	Ba, Be, Ga, Nb, Rb, Sc, Ta, LREE	Cs, Th	–
	ZOM 3	Be, Cs, Ga, Li, Nb, Ta, Th	Cu	–
	ZOM 4	Be, Ga, Li, Th	Cu	–
	ZOM 8	Be, Co, Ga, Mn	Li	–
	ZOM 9	Ba, Cs, Ga, Nb, Sc, Ta, HREE	Be, Rb, Th, LREE	–
Alandroal far from mineralization	ZOM 13	Ba, Be, Cs, Ga, Nb, Rb, Ta, Th, LREE	–	–
	ZOM 14	Be, Cr, Ga, Rb, LREE, HREE	V	–
Barrancos far from mineralization	ZOM 10	Ag, Pb, V, LREE	Sb	–
	ZOM 11	Be, Cr, Cu, Pb, Y, LREE	Ag, Sb, V, HREE	–
Miguel Vacas B1	1	–	–	–
	2$^+$	**Be, Ga, Li**	**–**	**–**
	3$^+$	**Be, Cs, Cu, Ga, Nb, Rb, Ta, Th, Zr, LREE, HREE**	**Cr, V**	**–**
	4$^+$	**Be, Cs, Ga, Rb, V, LREE**	**Cu**	**–**
	5	Be, Cs, Ga, Nb, Rb, Ta, Th	–	–
Miguel Vacas B2	1	Be, Ga, Li	–	–
	2	Be, Cr	V	–
	3	Ag, Be, Co, Cr, Se, HREE	Cu, Ni, V	–
	4	Be, LREE	V	–
	5$^+$	**Bi**	**–**	**–**
	6$^+$	**Be, Ga, Nb, Rb, Sc, Sn, Ta, Th, LREE**	**V**	
Miguel Vacas B3	1	Be, Cr, Ni, Rb, Sr, Y	Th, V, LREE, HREE	–
	2	Cr, Ni, LREE, HREE	As, Cu, Mo	V
	3	Be, Cr, Ga, Ni, Rb, Th, LREE, HREE	As, Cu, V	–
	4$^+$	**Bi, HREE**	**As, Cu, V, LREE**	**Ag**
	5$^+$	**As, Cr, LREE**	**Ag, Cu, V**	
Miguel Vacas B4	1	Be, Rb, V	–	–
	2	Cu, Ni, HREE	V	–
	3	Be, Cr, Cu, Mo, HREE	V, LREE	–
	4$^+$	**As, Be, Cs, Mn, Rb, Th**	**–**	**–**
	5$^+$	**As, Be, Rb, V**	**Mn**	**–**
	6$^+$	**As, Cu, Mo, LREE, HREE**	**V**	**–**
Miguel Vacas B5	1	Mo	V	–
	2$^+$	**Ag, Be, Bi, V**	**As**	**–**
	3	As, Mo, LREE, HREE	V	–
	4$^+$	**Be, Ga, Nb, Rb, Ta, Th**	**–**	**–**
	5$^+$	**Be, Bi, Cu, Ga, Nb, Rb, Ta, Th**	**LREE**	**–**
	6$^+$	**Be, Ga, Nb, Rb, Ta, Th, LREE**	**Sn**	**–**
	7$^+$	**Be, Mn**	**–**	**–**

The Cu profile also show great similarities with TOC, however the pattern is more variable. One meaningful feature of Cu pattern is the significative enrichment in Cu content around 50 m of drill cores (around 35 m deep), being highly pronounced in B1, B2, and B3 (Fig. 22), reaching values between 500 and 1000 ppm. In those samples, Cu have CC ranging between 2 and 10 as respect to BBS. Similar pattern is also noted in Fe content. Except for the B4, where the Fe content generally increase with depth, the other drill cores show higher concentration of Fe between 30 and 50 m deep (Figs. 22 and 23), sometimes with concordant increase of As (B5; Fig. 23). The high concentration of Cu and Fe at this depth can be related with post-depositional processes,

Table 5
Pearson correlation coefficients between selected elements.

	TOC	Al	Fe	K	P	S	Ti	Ag	As	Co	Cr	Cs	Cu	Mo	Nb	Ni	Pb	Sb	Sc	Th	U
TOC																					
Al	**−0.47**																				
Fe	−0.03	−0.01																			
K	−0.12	**0.51**	**−0.41**																		
P	**0.53**	−0.26	0.32	−0.08																	
S	**0.65**	**−0.45**	0.24	−0.31	**0.70**																
Ti	−0.30	**0.86**	**−0.35**	**0.63**	−0.24	**−0.47**															
Ag	−0.06	−0.27	0.05	−0.16	0.08	0.04	−0.28														
As	−0.08	**−0.39**	0.10	−0.19	0.04	0.00	**−0.42**	**0.70**													
Co	0.10	−0.05	**0.68**	−0.32	**0.52**	**0.51**	−0.22	0.11	0.02												
Cr	**0.65**	−0.22	0.12	0.07	**0.43**	**0.38**	−0.09	0.13	−0.03	0.21											
Cs	−0.17	**0.78**	−0.18	**0.42**	−0.16	−0.23	**0.74**	−0.13	−0.19	−0.17	0.07										
Cu	0.07	−0.15	0.09	−0.04	0.19	0.11	−0.09	0.34	**0.45**	0.26	0.23	0.09									
Mo	**0.41**	**−0.47**	−0.09	−0.23	0.05	**0.33**	**−0.38**	−0.04	0.30	−0.05	0.22	−0.23	**0.36**								
Nb	**−0.38**	**0.84**	−0.32	**0.66**	−0.31	**−0.54**	**0.95**	−0.26	**−0.41**	−0.25	−0.14	**0.59**	−0.11	**−0.38**							
Ni	**0.50**	−0.29	**0.44**	−0.27	**0.78**	**0.83**	−0.32	0.07	0.04	**0.73**	**0.43**	−0.19	0.35	0.27	**−0.37**						
Pb	**0.47**	**−0.46**	0.28	−0.30	**0.45**	**0.68**	**−0.41**	−0.05	−0.08	**0.44**	**0.49**	−0.33	0.04	0.29	**−0.46**	**0.64**					
Sb	**0.43**	**−0.58**	0.16	−0.29	**0.46**	**0.51**	**−0.47**	0.05	0.27	0.15	**0.54**	−0.27	0.20	**0.52**	**−0.54**	**0.56**	**0.69**				
Sc	−0.26	**0.91**	−0.03	**0.54**	−0.18	**−0.36**	**0.81**	−0.23	−0.30	−0.06	0.00	**0.80**	−0.15	−0.32	**0.78**	−0.21	**−0.37**	**−0.41**			
Th	−0.20	**0.72**	−0.14	**0.45**	−0.14	−0.17	**0.69**	−0.09	−0.20	−0.16	−0.09	**0.70**	−0.17	−0.25	**0.64**	−0.15	−0.21	−0.28	**0.80**		
U	**0.71**	**−0.50**	−0.06	−0.01	**0.41**	**0.57**	**−0.35**	0.13	0.28	0.02	**0.65**	−0.11	0.22	**0.60**	**−0.42**	**0.41**	**0.45**	**0.62**	−0.20	−0.12	
V	**0.58**	**−0.54**	−0.12	−0.17	0.29	0.33	**−0.34**	0.20	0.27	−0.05	**0.66**	−0.17	0.38	**0.69**	**−0.37**	0.29	0.32	**0.61**	−0.31	−0.24	**0.73**

Table 6
Ratio of selected redox sensitive elements for the studied samples (values corresponding to anoxic depositional conditions in bold).

	Samples	Ni/Co	V/Cr	Th/U
Alandroal	ZOM 1	2.60	1.79	4.63
Near mineralization	ZOM 2	4.44	**2.26**	12.4
	ZOM 3	4.83	1.79	6.09
	ZOM 4	8.32	1.60	5.41
	ZOM 8	1.20	1.38	5.94
	ZOM 9	7.19	1.62	12.6
Alandroal	ZOM 13	9.27	1.63	6.00
Far from mineralization	ZOM 14	5.74	**5.44**	2.79
Barrancos	**ZOM 10**	**34.8**	**16.5**	**0.38**
Far from mineralization	**ZOM 11**	**9.44**	**7.34**	**0.77**
Miguel Vacas	1	3.51	**3.63**	3.43
	2	3.48	1.51	6.36
B1	**3**$^{+}$	**23.1**	**7.41**	**1.12**
	4^{+}	**6.43**	**3.75**	**1.20**
	5^{+}	5.02	**2.48**	2.51
Miguel Vacas	1	5.14	**2.25**	1.44
	2	**14.9**	**11.9**	**1.44**
B2	**3**	**9.60**	**4.38**	**0.95**
	4	**9.45**	**6.17**	**1.17**
	5^{+}	**10.3**	**12.3**	**0.86**
	6^{+}	**9.40**	**7.55**	**1.09**
Miguel Vacas	**1**	**10.5**	**10.2**	**1.12**
	2	**16.8**	**24.7**	**0.46**
B3	3	5.81	**9.04**	1.68
	4^{+}	4.49	**10.6**	1.18
	5^{+}	4.86	**16.5**	0.76
Miguel Vacas	**1**	**23.0**	**4.58**	**1.46**
	2	**16.8**	**16.5**	**0.72**
B4	**3**	**11.1**	**7.71**	**0.43**
	4^{+}	4.49	**2.24**	2.21
	5^{+}	5.79	**4.74**	0.82
	6^{+}	**13.0**	**9.09**	**0.69**
Miguel Vacas	**1**	**12.4**	**15.9**	**0.86**
B5	**2**$^{+}$	**16.1**	**5.85**	**0.68**
	3	4.80	**10.6**	0.57
	4^{+}	6.58	1.98	6.32
	5^{+}	4.20	**2.82**	4.27
	6^{+}	5.58	1.83	5.38
	7^{+}	2.73	1.97	2.94

denoting the transition from oxidizing to reducing conditions (see also section 5.5.2.; Fig. 25).

The paleoredox ratios (Th/U and Ni/Co) also show significative variations compatible with variations of TOC. Indeed, the increase of TOC values is consistent with the increase of Ni/Co ratio and the decrease of Th/U ratio (Figs. 22 and 23), denoting the preservation of organic matter during sedimentation of black shales in anoxic environment.

The paleotemperatures show an irregular pattern with the depth, which may indicate the presence of hydrothermal fluids (e.g., Barker, 1991; Glikson and Mastalerz, 2000), promoting discrepant thermal evolution of organic matter in black shales. Thus, the pathway of hydrothermal fluids associated to mineralized Cu veins contributed to the discrepant maturation of organic matter, due to the percolation of the intermediate to high temperatures of fluids (Maia et al., 2019), and for the precipitation of metals, including those that are scattered in the host rocks.

Considering these results (Fig. 22 and 23) together with the mineralogical information (Table S4 in supplementary material), and the available bibliographic data with the description of the Cu deposit in the studied area (e.g., Fernandes, 2012; Mateus et al., 2013; Maia et al., 2020), it is possible to discuss the relation between all the parameters. Samples collected between 35 m to 50 m depth have, in general, an enrichment in Fe, As, Cr, Cu, Ni, U, V, and REE, together with the highest TOC and S values (Table 4; Fig. 22 and 23). This could indicate that these black shales were not primary enriched in metals but were enriched during post-depositional processes.

6.5. Sousel-Barrancos metallogenic belt ores and the Miguel Vacas Cu deposit genesis

6.5.1. Discussing the regional scale ore deposits

The genesis of Cu deposits from Sousel-Barrancos metallogenic belt is not consensual. Two hypotheses were raised based on previous studies:

(1) Several authors (e.g., Mateus et al., 2003, 2013; Tornos et al., 2004; Fernandes, 2012) suggest that the Cu content of Sousel-Barrancos ores was remobilized from Paleozoic metasediments, through hydrothermal chemically modified meteoric waters and residual metamorphic fluids, and later precipitated in vein type structures. According to Mateus et al. (2003, 2013), the host Paleozoic rocks are pre-enriched in base metals. Other authors (e.g., Piçarra, 2000; Roseiro et al., 2020) also emphasizes that Silurian metasedimentary units were deposited in anoxic to euxinic depositional environment, which benefited Cu preconcentration as sulfide phases, or in organic matter by chelation.

(2) Recently, Maia et al. (2019, 2020) propose a revised model for Sousel-Barrancos metallogenic belt Cu-deposits, stating that the fluids found in the Mociços and other Cu-deposits in the region could be linked with a deep-seated magmatic body, that may be similar to other Late Carboniferous-Permian calc-alkaline igneous bodies of the OMZ (e.g., Santa Eulália Igneous Complex or the Alcáçovas - Baleizão porphyries). According to these authors, this deep-seated magmatic body is as possible source of hydrothermal fluids and possibly metals for Sousel-Barrancos metallogenic belt Cu-deposits. Although, the authors do not exclude the possibility of Paleozoic metasedimentary units also contributed as metal source in the Sousel-Barrancos ore deposits.

The data herein presented show an irregular maturation of organic matter (Table 2, Fig. 19 and 20) and concentration in elements patterns (Fig. 21, 22 and 23) at regional scale, both in the outcrop and drill core samples. As aforementioned, paleotemperatures obtained using the random mean reflectance values, indicate discrepant maturation of the organic matter particles along the Miguel Vacas drill cores, with temperature between 230 °C and 345 °C. This indicates that the maturation of the organic matter is not totally dependent of regional metamorphism and could be explained by the circulation of hydrothermal fluids of intermediate temperatures, associated with the formation of mineralized veins, in accordance with previous mentioned models (Maia et al., 2019; Laranjeira et al., 2019).

According to bibliographic data, the regional metamorphism in the Sousel-Barrancos Metallogenic Belt do not exceed the chlorite-biotite zones in the greenschist facies conditions (Perdigão et al., 1982; Oliveira, 1984; Pereira et al., 2012; Moreira et al., 2019), which is also in accordance with reflectance data obtained for the shale-derived rocks in the core of Estremoz Anticline (Laranjeira et al., 2023b), and with general values of reflectance and paleotemperatures presented in this study. However, the spatial variance of reflectance values indicate discrepant spatial evolution. The refletance values reveal that the maturation of organic matter in samples from Alandroal and Barrancos is generally higher (Rr between 3.0% to 4.5% and R_{max} between 5.0% to 6.5%) than samples from Miguel Vacas, collected along different drill cores, with the exception of samples B3_2 and B5_5. The spatial analysis within Alandroal area shows that values obtained in the Mociços region (Rr between 3.9% to 4.3% and R_{max} between 6.9% to 7.7%) are higher than: in Ferrarias (samples ZOM 8 and ZOM 9, Rr between 3.7% to 3.9% and R_{max} between 6.4% to 7.1%); the distal areas from mineralizations located at West near Estremoz Anticline (Rr between 3.0% to 3.9% and R_{max} between 5.0% to 6.5%); and, values obtained in all samples from Miguel Vacas (Rr between 1.7% to 4.7% and R_{max} between 2.3% to 6.7%) (Fig. 24). As respect to Barrancos region, the obtained data reveal higher values of refletance at NE ($VR_{r\text{-}eq}$ 4.15% and $VR_{max\text{-}eq}$ 5.31%), than in the SW sample (ZOM 11; $VR_{r\text{-}eq}$ 3.13% and $VR_{max\text{-}eq}$ 4.86%). This can be the result of differential thermal evolution of organic matter associated with spatial arrangement of regional and/or thermal metamorphism during the late tectono-metamorphic episodes of Variscan Cycle.

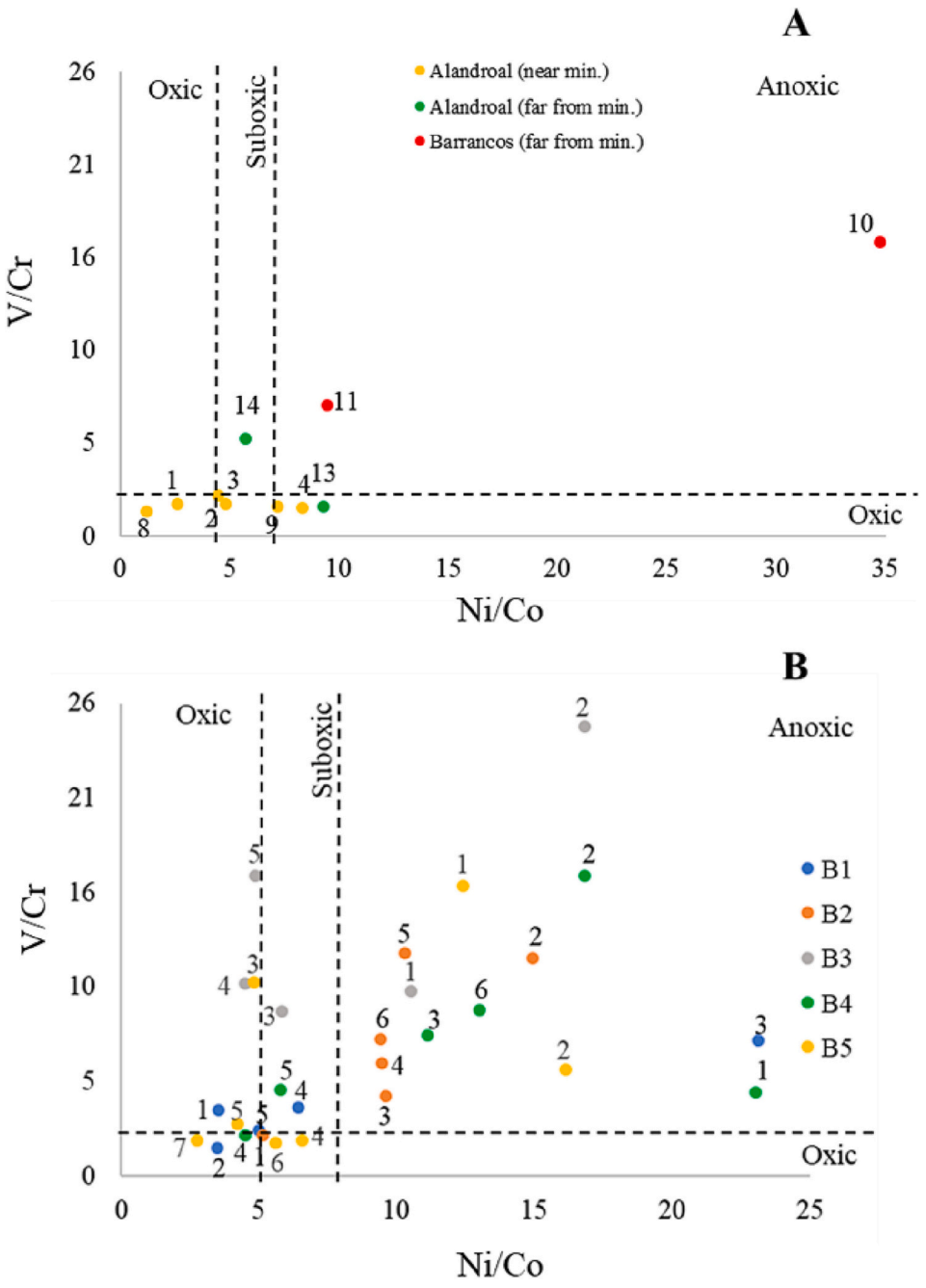

Fig. 20. Cross plot of trace element ratios used as paleoredox proxies (adapted from Rimmer, 2004). Ranges for V/Cr and Ni/Co are from Jones and Manning (1994). A) Samples from outcrops; B) Samples from Miguel Vacas drill cores.

A possible presence of a deep-seated magmatic body controlling the late Paleozoic thermal evolution of Sousel-Barrancos Metallogenic Belt, as proposed by Maia et al. (2020), could explain this spatial variation of maturation at regional scale (Fig. 24), but also: (1) the presence of a thermal metamorphism halo associated to an intense hydrothermal alteration in Zahinos and Oliva de la Frontera region; (2) the magnetic anomaly and the pseudo susceptibility pattern in Portugal and Spain, showing the presence of positive anomalies (e.g., Silva et al., 2000); (3) values of electrical resistivity model obtained by Almeida et al. (2001), which shows an intense and shallow anomaly underneath near the Mociços area; and (4) the nature of hydrothermal fluids associated to the Cu occurrences along this metallogenic belt (Maia et al., 2020). Therefore, organic matter reflectance data in Alandroal region seems to show a general increase of reflectance from NW to SE, toward the main anomaly of Zahinos-Oliva de la Frontera region (Fig. 24). Although with a smaller dataset, the spatial evolution of Barrancos region appears to show similar pattern with increase of paleotemperatures toward NE.

Local factors can also inluence the thermal maturation of organic matter. Indeed, the samples from Ferrarias are located close to the Messejana fault (Fig. 24), where Mesozoic age doleritic rocks are described (Schermerhorn et al., 1978), explaining the higher maturation in this region. In Barrancos region (extending up until Mociços area), a igneous complex characterized by an association of lithologies comprising felsic and mafic volcanics, carbonates, and synsedimentary breccias are also described (Perdigão et al., 1982; Piçarra, 2000). The age of Barrancos Igneous Complex is unknown, but it is atribbuted to Upper Paleozoic.

However, there is also a considerable discrepancy between the

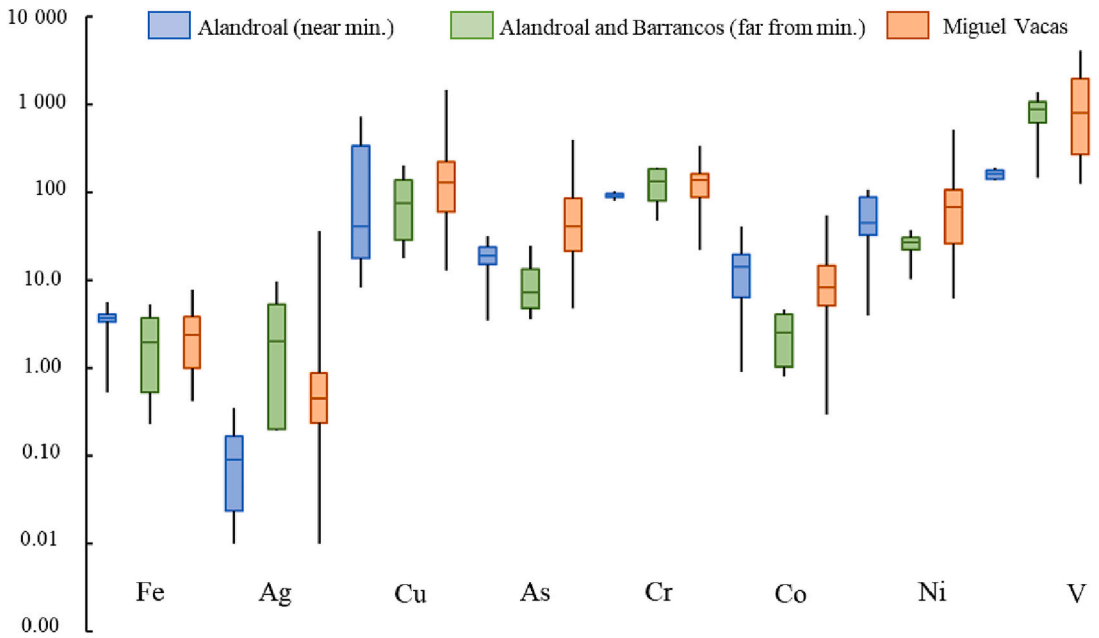

Fig. 21. Boxplots for Fe (%), Ag, As, Co, Cr, Cu, Ni, and V (ppm) content of outcrop and drill core samples.

values of reflectance (both Rr and R_{max}) in the outcrop samples from Alandroal area (nearest to mineralization) and in several samples from Miguel Vacas drill cores (Fig. 18), which cannot be explained by the previous described spatial variation of regional metamorphism effect. Indeed, fluid inclusion studies both in Mociços (Maia et al., 2019, 2020) and Migues Vacas (Maia et al., 2019) deposits allow to constrain the minimum trapping temperatures of hidrothermal fluids associated with both deposits, showing a range of temperatures between 240 °C and 420 °C to Mociços, and between 180 °C and 350 °C to Miguel Vacas Cu vein deposit. These temperatures are consistent with maximum values of paleotemperatures estimated based on the reflectance of organic matter in the studied samples.

Therefore, the thermal maturation of the black shales from Sousel-Barrancos Metallogenic Belt seems be related with hydrothermal metamorphism, possibly associated with the deep-seated magmatic body as proposed by Maia et al. (2020). This magmatic body should be responsible for the P-T conditions during late tectono-metamorphic stages of the Variscan Cycle in this metallogenic belt and for supplying the hypersaline hydrothermal fluids responsible by the diferential thermal maturation of organic matter associated with fluid circulation along host rocks, and probably associated with brittle-ductile Cu vein emplacement.

6.5.2. *Supergenic and primary enrichments domains in Miguel Vacas*

The Miguel Vacas ancient mine is a Cu-rich vein crosscutting Silurian black shales (Mateus et al., 2003, 2013), where distinct vertical domains are identified (e.g., Fernandes, 2012; Mateus et al., 2003, 2013), from the surface zone to the deeper one (Fig. 25):

- Surface zone, characterized by Fe and Mn oxides and hydroxides accompanied by quartz evidencing strong oxidation; the abundant Fe oxides and hydroxides are the result of the leaching of the primary sulfides (chalcopyrite, pyrite, and arsenopyrite) by the acidic and oxidizing conditions assisted by the meteoric water, which destabilize and deplete this zone of Cu phases.

- Supergene enrichment zone that results from the reprecipitation of the leached Cu from the surface zone; the leached Cu occurs in two different forms (Guilbert and Park, 1986; Chávez, 2000; Robb, 2005; Sillitoe, 2005; Pohl, 2011): (1) in the more oxidizing domain, the ores are composed by secondary Cu minerals (oxides, carbonates, phosphates, sulfates) and Fe oxides, and (2) in the more reducing conditions, secondary Cu sulfides such as chalcocite, covellite and bornite occur, being accompanied by primary sulfides such as chalcopyrite, pyrite and arsenopyrite.

- Primary deposit domain, which mainly contains chalcopyrite, pyrite and arsenopyrite with no traces of alteration or secondary mineralization, such as secondary Fe and Cu phases.

Therefore, it is assumed that the primary mineralization results from the circulation of hydrothermal fluids, independently of their nature, not excluding the hypothesis that those fluids might remobilize metals from the surrounding rocks (Mateus et al., 2003, 2013; Fernandes, 2012; Maia et al., 2020). Presented data shows that there are some primary sulfides phases associated with organic matter, for example pyrite, chalcopyrite and arsenopyrite that were identified in petrographic studies. Additionally, no significant enrichment in Cu and other metals in the background samples were found. In the same way, our data does not exclude a hydrothermal fluid primary enriched in metals.

This Fe + Cu ± As ± Ag rich hydrothermal fluid, in favorable physical and chemical conditions, generates the primary sulfides phases, probably associated with the brittle fracture zones (e.g., Mociços and Miguel Vacas) during the late Variscan deformation event (Maia et al., 2020). In this case, the black shales, more specifically the organic matter and the associated S, can act as a redox changing environment promoting the precipitation of primary metallic sulfide phases (Pasava et al., 2008).

Afterwards, the meteoric-derived fluids remobilize metals from the vein, but also from Silurian host rock formations in the most superficial oxidizing zones. As such, Cu is remobilized from superficial zones and transported to deeper ones, but Fe will be concentrated in the Gossan zone as iron oxides and hydroxides (Fig. 25). In depth, the redox conditions change, and Cu finds the optimal conditions to reprecipitate as secondary Cu minerals. In the studied samples, the enriched Cu black shales were identified between 35 and 50 m deep (50 to 70 m in the drill cores), probably corresponding to the transition between surface oxidizing zone and the reducing zone (Fig. 25). Sometimes very close to the oxidation-reduction zone (equivalent to around 35 m to 50 m deep), some Ag-rich levels are also locally found. This behavior was also described in previous investigations for other enrichment type deposits (e.g., Velasco et al., 2013). The Ag content in analyzed black shales has high correlation coefficient with As (Table 5), allowing to consider its association with the presence of sulfides as arsenopyrite or arsenic

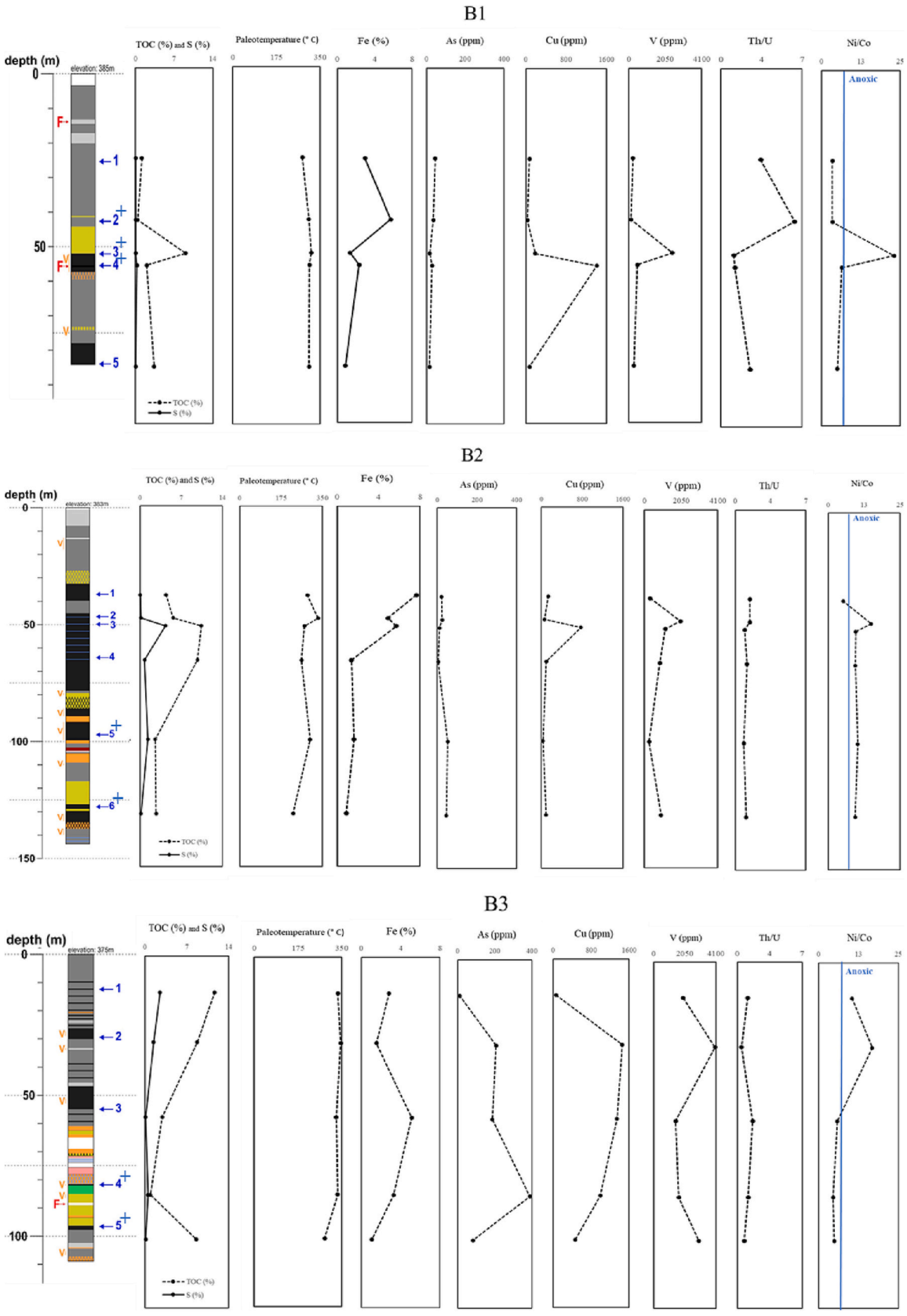

Fig. 22. Vertical variations of TOC, S, paleotemperatures, Fe As, Cu and paleoredox ratios Th/U and Ni/Co from B1, B2 and B3 drill cores.

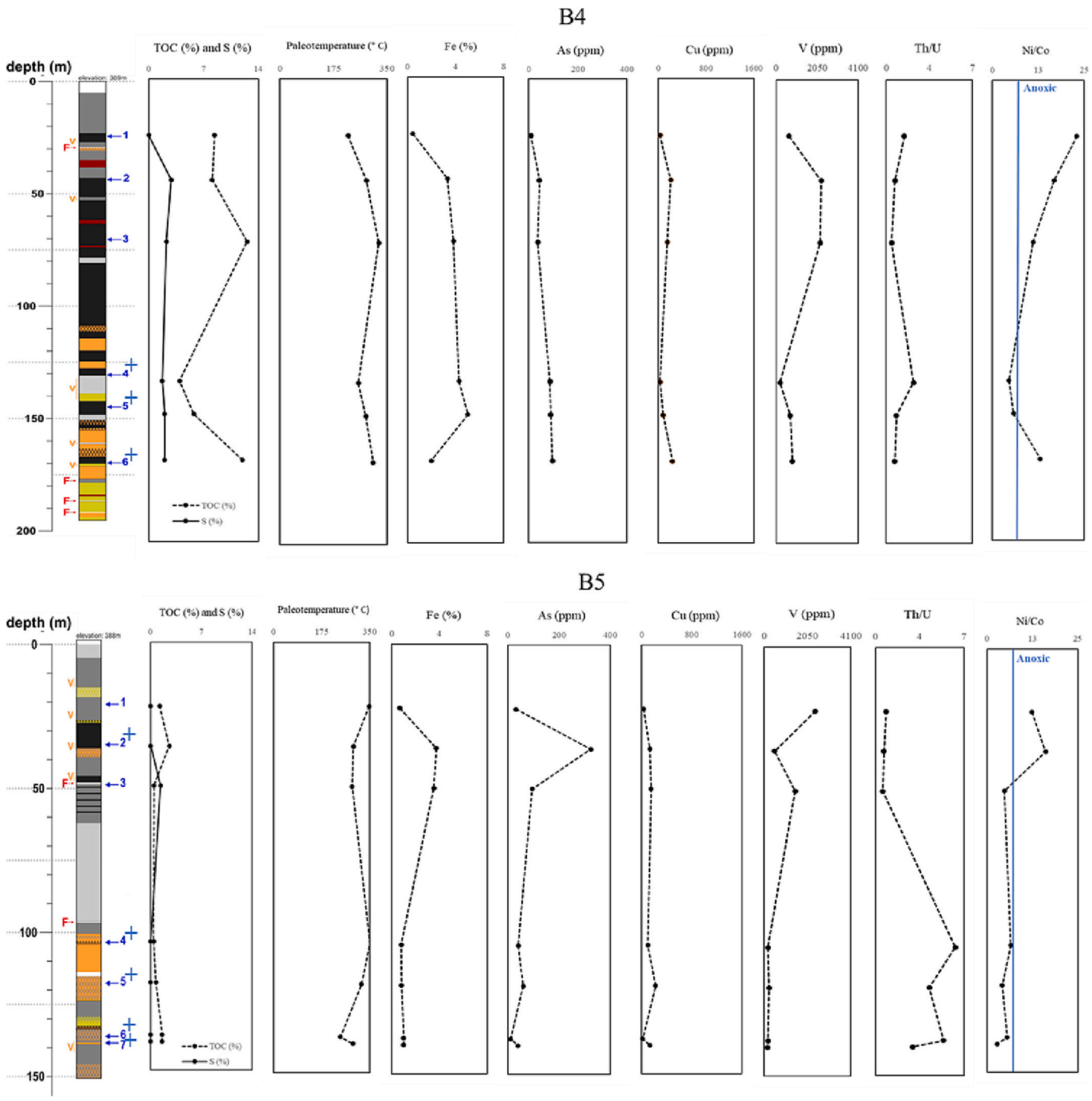

Fig. 23. Vertical variations of TOC, S, paleotemperatures, Fe As, Cu and paleoredox ratios Th/U and Ni/Co from drill cores B4 and B5.

pyrite.

Consequently, a portion of Cu was removed from the mineralized veins, which were in an oxidizing environment, and was transported by meteoric-derived fluids and re-precipitated under reducing conditions, in the form of secondary Cu phases, as previously reported (Fernandes, 2012).

7. Conclusions

Samples of Silurian black shales from OMZ, spatially associated with Cu mineralizations in Sousel-Barrancos metallogenic belt, were studied through petrography, mineralogy, and geochemistry to understand their relationship with processes that led to the formation of ore deposits, highlighting the role of organic matter.

Redox sensitive proxies indicate that almost all black shale samples were deposited in suboxic to anoxic environmental conditions. The Pearson correlation coefficient between TOC and S with metals as Fe, Cu, As and Ag suggests that those elements are not primary related with organic matter. A higher level of Cu enrichment was identified in some black shale samples collected in drill cores intercepting the Miguel Vacas Cu vein, being probably related with supergene enrichment processes. In Miguel Vacas, the Cu enrichment domain, together with the irregular maturation profiles, point to the transition between superficial zone and the supergene enrichment zone around 35 to 50 m depth. The samples corresponding to these levels also present, in general, an enrichment in some other elements, together with higher concentrations of TOC and S

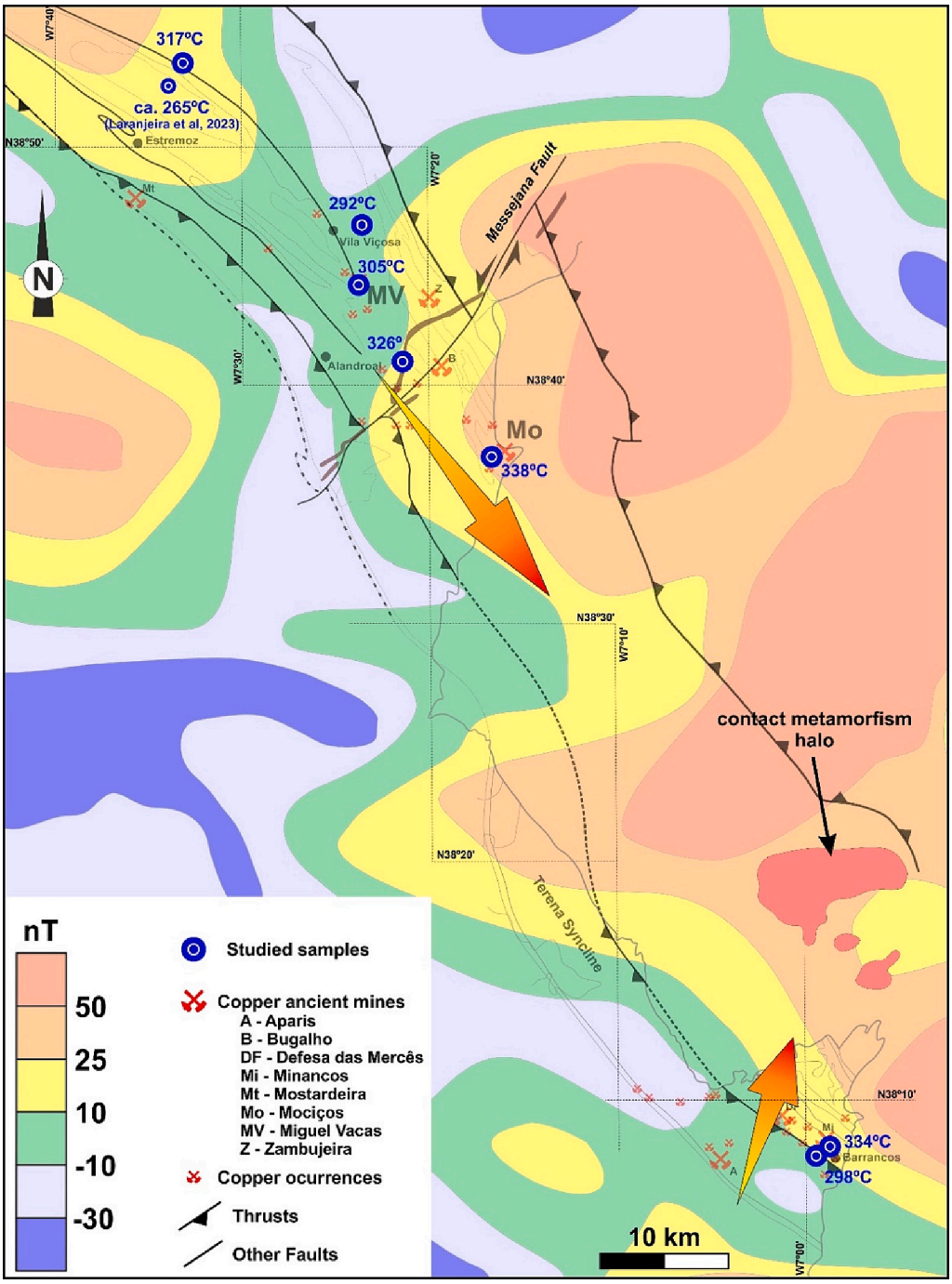

Fig. 24. Spatial disposition of black shale samples and the calculated paleotemperatures, overlaid to the magnetic anomaly pattern of Portugal and Spain (adapted from Silva et al., 2000).

that could be indicative that the black shales were not primary enriched in metals but were enriched during post-depositional processes.

The obtained results also indicated that the variation of thermal maturation in outcrop and drill core samples from Alandroal (including Miguel Vacas Cu deposit) and Barrancos regions can be interpreted as a result of the hydrothermal metamorphism. In the drill core samples from Miguel Vacas, it was identified an irregular profile of thermal maturation of organic matter associated to the pathway of hydrothermal fluids. The regional thermal evolution shows a spatial architecture compatible with the existence of a deep-seated magmatic body, as previously proposed by other authors, probably emplaced during late Variscan stages, which possibly generates magmatic-derived hydrothermal fluids responsible for the Sousel-Barrancos Cu deposits.

CRediT authorship contribution statement

In this document is explicit the authors individual contributions to the paper using the relevant CRediT (Contributor Roles Taxonomy) roles:

i. **Vanessa Laranjeira:** conceptualization, methodology, formal analysis, investigation, and writing - original draft.
ii. **Joana Ribeiro:** conceptualization, supervision and writing - review and editing.

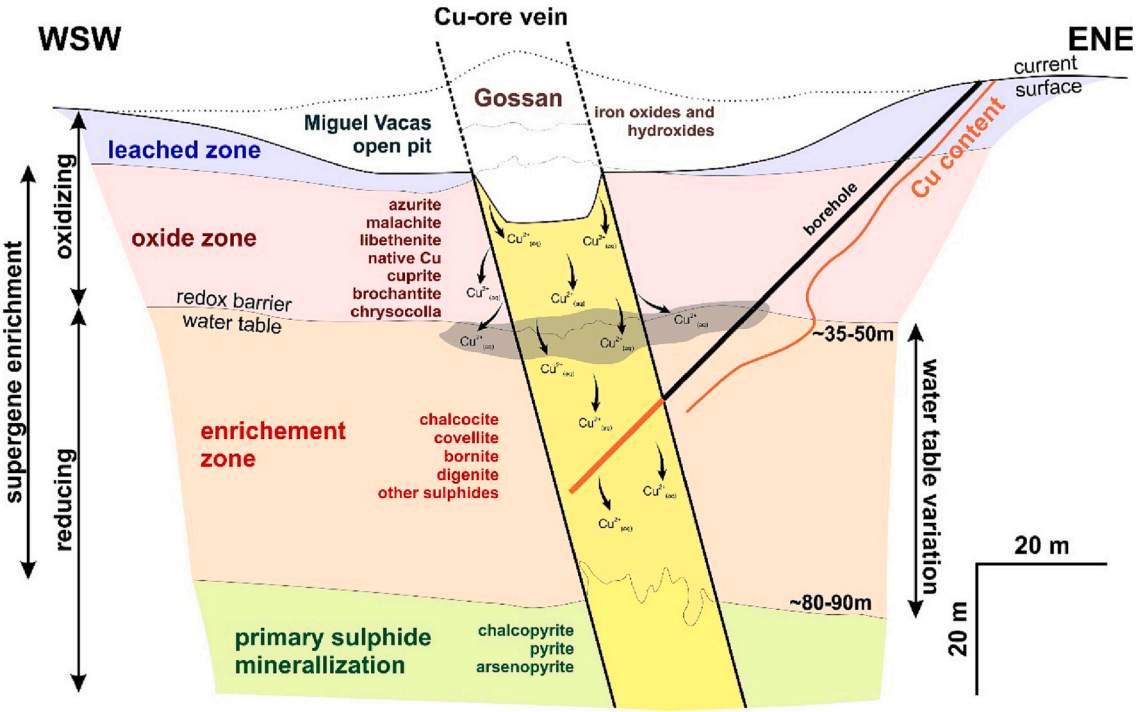

Fig. 25. Schematic cross section of Miguel Vacas ancient mine, emphasizing the distinct ore minerals in depth and the oxidizing and reducing domains (general model adapted from Pohl, 2011 and Fernandes, 2012).

iii. **Noel Moreira:** conceptualization, resources and writing - review and editing.
iv. **Pedro Nogueira:** resources and writing - review and editing.
v. **João Graciaço Mendonça Filho:** resources - review and editing.
vi. **Fernando Rocha:** resources - review and editing.
vii. **Deolinda Flores:** supervision and writing - review and editing.

Declaration of Competing Interest

The authors declare that they have no known competing financial interests or personal relationships that could have appeared to influence the work reported in this paper.

Data availability

Data will be made available on request.

Acknowledgements

This work is supported by national funding awarded by FCT - Foundation for Science and Technology, I.P., projects UIDB/04683/2020 and UIDP/04683/2020. V. Laranjeira thanks the funding of the PhD scholarship (SFRH / BD / 137567/2018) awarded by FCT and the EU, through national funds and the European Social Fund (ESF). N. Moreira and P. Nogueira acknowledge the contribution of the project ZOM-3D (ALT20-03-0145-FEDER-000028), funded by Alentejo 2020 through the FEDER/FSE/FEEI.

Appendix A. Supplementary data

Supplementary data to this article can be found online at https://doi.org/10.1016/j.coal.2023.104253.

References

Almeida, E., Pous, J., Monteiro, Santos F., Fonseca, P., Marcuello, A., Queralt, P., Nolasco, R., Mendes-Victor, L., 2001. Electromagnetic imaging of a compressional tectonic in SW Iberia. Geophys. Res. Lett. 28, 439–442. https://doi.org/10.1029/2000GL012037.

Araújo, A., Piçarra, J.M., Borrego, J., Pedro, J., Oliveira, J.T., 2013. As Regiões Central e sul da Zona de Ossa-Morena. In: de Portugal, Geologia, Dias, R., Araújo, A., Terrinha, P., Kullberg, J.C. (Eds.), Mineralizações no sector português da Zona de Ossa-Morena, pp. 577–619.

ASTM D 7708-14, 2014. Standard Test Method for Microscopical Determination of the Reflectance of Vitrinite Dispersed in Sedimentary Rocks. ASTM International, p. 10.

Barker, C.E., 1991. Implications for organic maturation studies of evidence for a geologically rapid increase and stabilization of vitrinite reflectance at peak temperature: Cerro Pieto geothermal system. Associat. Petrol. Geol. Bull. 75, 1852–1863.

Barker, C.E., Pawlewicz, M.J., 1994. Calculation of vitrinite reflectance from thermal histories and peak temperatures - a comparison of methods. In: Mukhopadhyay, P.K., Dow, W.G. (Eds.), Vitrinite Reflectance as a Maturity Parameter. Applications and Limitations. *In:* Symposium Series 570, vol. DC. American Chemical Society, Washington, pp. 216–229. https://doi.org/10.1021/bk-1994-0570.ch014.

Bertrand, R., 1990. Correlations among the reflectances of vitrinite, chitinozoans, graptolites and scolecodonts. Org. Geochem. 15, 565–574.

Boyong, Y., Bin, H., Zhengyu, B., Zhaogan, Z., 2011. REE geochemical characteristics and depositional environment of the black shale-hosted Baiguoyuan Ag-V deposit in Xingshan, Hubei Province, China. J. Rare Earths 29 (5), 499–506.

Chávez, W., 2000. Supergene oxidation of copper deposits: zoning and distribution of copper oxide minerals. Soc. Econ. Geol. Newsletter 41 (1), 10–21.

Cooper, R.A., Rigby, S., Loydell, D.K., Bats, D.E.B., 2012. Palaeoecology of the graptoloidea. Earth Sci. Rev. 112, 23–41. https://doi.org/10.1016/j.earscirev.2012.01.001.

Corrula, L.M., Branco, J.M.C., 2005. Área do Alandroal: Relatório do primeiro semestre de 2005 (Rio Narcea Gold Mines, S.a. - Sucursal em Portugal). In: International Report, LNEG, Lisbon (not published).

Coveney, R.M., Pašava, J., 2004. Special issue on black shales and related mineral deposits. Ore Geol. Rev. 1-2, 167 pp.

Dai, S., Li, T., Jiang, Y., Ward, C.R., Hower, J.C., Sun, J., Liu, J., Song, H., Wei, J., Li, Q., Xie, P., 2015. Mineralogical and geochemical compositions of the Pennsylvanian coal in the Hailiushu Mine, Daqingshan Coalfield, Inner Mongolia, China: implications of sediment-source region and acid hydrothermal solutions. Int. J. Coal Geol. 137, 92–110. https://doi.org/10.3390/min8030104.

Dai, S., Graham, I.T., Ward, C.R., 2016. A review of anomalous rare earth elements and yttrium in coal. Int. J. Coal Geol. 159, 82–95. https://doi.org/10.1016/j.coal.2016.04.005.

Dill, H., 1986. Metallogenesis of early Paleozoic graptolite shales from the Graefenthal Horst (Northern Bavaria - Federal Republic of Germany). Econ. Geol. 81, 889–903. https://doi.org/10.2113/gsecongeo.81.4.889.

Disnar, J.R., Sureau, J.F., 1990. Organic matter in ore genesis: Progress and perspectives. Org. Geochem. 16 (1–3), 577–599. https://doi.org/10.1016/0146-6380(90)90072-8.

Eakin, P.A., Gize, A.P., 1992. Reflected-light microscopy of uraniferous bitumens. Mineral. Mag. 56, 85–99. https://doi.org/10.1180/minmag.1992.056.382.11.

El-Anwar, E.A.A., Mekky, H.S., Wahab, W.A., 2018. Geochemistry, mineralogy and depositional environment of black shales of the Duwi Formation, Qusseir area, Red Sea coast, Egypt. In: Carbonates and Evaporites, 34. Springer, pp. 883–892. https://doi.org/10.1007/s13146-017-0417-7.

Emerson, S.R., Huested, S.S., 1991. Ocean anoxia and the concentrations of molybdenum and vanadium in seawater. Mar. Chem. 34, 177–196. https://doi.org/10.1016/0304-4203(91)90002-E.

Eric, B.E., Philip, F., Emile, E., Isaac Konfor, N., Salomon Betrant, B., Daniel Florent, A., Bessa Armel Zacharie, E., 2019. Geochemical characteristics of shales in the Mamfe Basin, South West Cameroon: implication for depositional environments and oxidation conditions. J. Afr. Earth Sci. 149, 131–142. https://doi.org/10.1016/j.jafrearsci.2018.08.004.

Fernandes, G., 2012. Mineralizações de Cobre da Mina de Miguel Vacas: Caracterização Petrográfica e Geoquímica. Master thesis.. Faculty of Sciences of the University of Lisbon, 345 pp.

Finkelman, R.B., Palmer, C.A., Wang, P., 2018. Quantification of the modes of occurrence of 42 elements in coal. Int. J. Coal Geol. 185, 138–160. https://doi.org/10.1016/j.coal.2017.09.005.

Galarraga, F., Reategui, K., Martïnez, A., Martínez, M., Llamas, J.F., Marquez, G., 2008. V/Ni ratio as a parameter in palaeoenvironmental characterisation of nonmature medium-crude oils from several Latin American basins. J. Pet. Sci. Eng. 61, 9–14. https://doi.org/10.1016/j.petrol.2007.10.001.

Gize, A.P., 1993. The analysis of organic matter in ore deposits. In: Parnell, J., Kucha, H., Landais, P. (Eds.), Bitumens in Ore Deposits: Special Publication on the Society for Geology Applied to Mineral Deposits. Springer-Verlag, pp. 28–52. https://doi.org/10.1007/978-3-642-85806-2_3.

Glikson, M., Mastalerz, M., 2000. Organic Matter and Mineralisation: Thermal Alteration, Hydrocarbon Generation and Role in Metallogenesis. Springer Dordrecht, p. 454. https://doi.org/10.1007/978-94-015-9474-5.

Gonçalves, P.A., Pinheiro, S., Mendonça Filho, J.G., Mendonça, J.O., Flores, D., 2020. Study of a Silurian sequence of Dornes region (Central Iberian Zone, Portugal): the contribution of organic petrology and palynofacies. Int. J. Coal Geol. 225, 103501 https://doi.org/10.1016/j.coal.2020.103501.

Goodarzi, F., 1984. Organic petrography of graptolite fragments from Turkey. Mar. Pet. Geol. 1, 202–210. https://doi.org/10.1016/0264-8172(84)90146-6.

Goodarzi, F., 1985. Dispersion of optical properties of graptolite epiderms with increased maturity in early Paleozoic organic-rich sediments. Fuel 64, 1735–1740. https://doi.org/10.1016/0016-2361(85)90401-6.

Goodarzi, F., Norford, B.S., 1987. Optical properties of graptolite epiderma review. Bull. Geol. Soc. Denmark 35, 141–147.

Goodarzi, F., Gentzis, T., Harrison, C., Thorsteinsson, R., 1992. The significance of graptolite reflectance in regional thermal maturity studies, Queen Elizabeth Islands, Arctic Canada. Org. Geochem. 18, 347–357. https://doi.org/10.1016/0146-6380(92)90075-9.

Greenwood, P.F., Brocks, J.J., Grice, K., Schwark, L., Jaraula, C.M.B., Dick, J.M., Evans, K.A., 2013. Organic geochemistry and mineralogy. I. Characterization of organic matter associated with metal deposits. Ore Geol. Rev. 50, 1–27. https://doi.org/10.1016/j.oregeorev.2012.10.004.

Guilbert, J.M., Park, C.F., 1986. The Geology of Ore Deposits. W.H. Freeman and Company, New York, p. 985.

Hackley, P.C., Guevara, E.H., Hentz, T.F., Hook, R.W., 2009. Thermal maturity and organic composition of Pennsylvanian coals and carbonaceous shales, north-Central Texas: implications for coalbed gas potential. Int. J. Coal Geol. 77, 294–309.

Hartkopf-Fröder, C., Königshof, P., Littke, R., Schwarzbauer, J., 2015. Optical thermal maturity parameters and organic geochemical alteration at low grade diagenesis to anchimetamorphism: a review. Int. J. Coal Geol. 150-151, 74–119. https://doi.org/10.1016/j.coal.2015.06.005.

Hatch, J.R., Leventhal, J.S., 1992. Relationship between inferred redox potential of the depositional environment and geochemistry of the upper Pennsylvanian (Missourian) stark shale member of the Dennis Limestone, Wabaunsee County, Kansas, USA. Chem. Geol. 99, 65–82. https://doi.org/10.1016/0009-2541(92)90031-Y.

Hunt, J.M., 1996. Petroleum Geochemistry and Geology (2nd Eds). W. H. Freeman and Company, New York, p. 743.

ISO 7404-2, 2009. Methods for the Petrographic Analysis of Coals - Part 2: Methods of Preparing Coal Samples, 12 pp.

Jones, B., Manning, D., 1994. Comparison of geochemical indices used for the interpretation of palaeoredox conditions in ancient mudstones. Chem. Geol. 111, 111–129. https://doi.org/10.1016/0009-2541(94)90085-X.

Ketris, M.P., Yudovich, Y.E., 2009. Estimations of Clarkes for Carbonaceous biolithes: World averages for trace element contents in black shales and coals. Int. J. Coal Geol. 78, 135–148. https://doi.org/10.1016/j.coal.2009.01.002.

Kwiecinska, B., Petersen, H.I., 2004. Graphite, semi-graphite, natural coke, and natural char classification-ICCP system. Int. J. Coal Geol. 57, 99–116. https://doi.org/10.1016/j.coal.2003.09.003.

Landais, P., 1993. Bitumens in uranium deposits. In: Parnell, J., Kucha, H., Landais, P. (Eds.), Bitumens in Ore Deposits: Special Publication on the Society for Geology Applied to Mineral Deposits, 9, pp. 213–235.

Laranjeira, V., Ribeiro, J., Moreira, N., Nogueira, P., Mendonça Filho, J.G., Flores, D., 2019. Caraterização geoquímica da matéria orgânica de xistos negros associados a mineralização de Cu na Zona Ossa Morena. In: Extended abstracts XII Iberian Congress of Geochemistry, pp. 187–190.

Laranjeira, V., Ribeiro, J., Moreira, N., Nogueira, P., Flores, D., 2023a. Geochemistry of Precambrian black shales from Ossa-Morena Zone (Portugal): depositional environment and possible source of metals. J. Iber. Geol. https://doi.org/10.1007/s41513-022-00202-6.

Laranjeira, V., Ribeiro, J., Moreira, N., Nogueira, P., Mendonça Filho, J.G., Flores, D., 2023b. Petrographic and geochemical characterization of organic matter in Precambrian black shales from Ossa-Morena Zone, South of Portugal. In: Chaminé, H.I., Fernandes, J.A. (Eds.), Advances in Geoengineering, Geotechnologies, and Geoenvironment for Earth Systems and Sustainable Georesources Management - Proceedings of the 1st Conference on Georesources, Geomaterials, Geotechnologies and Geoenvironment (4GEO). Springer ASTI Series (in press).

Leventhal, J.S., 1986. Roles of organic matter in ore deposits. In: Dean, W.E. (Ed.), Organics and Ore Deposits. Denver Regional Exploration Society, Denver, Colorado, pp. 7–20. https://doi.org/10.1007/978-1-4615-2890-6_25.

Leventhal, J., 1993. Metals and black shales. In: Engel, M.H., Macko, S.A. (Eds.), Organic Geochemistry - Principles and Applications. Plenum Press, New York, pp. 581–592. https://doi.org/10.1007/978-1-4615-2890-6.

Li, J., Qin, Y., Chen, Y., Shen, J., 2022. Microstructural characteristics of graphite microcrystals in graphitized coal: insights from petrology, mineralogy and spectroscopy. Minerals 12, 1189. https://doi.org/10.3390/min12101189.

Liu, J., Yang, Z., Yan, X., Ji, D., Yang, Y., Hu, L., 2015. Modes of occurrence of highly-elevated trace elements in superhigh-organic-sulfur coals. Fuel 156 (15), 190–197.

LNEG, 2010. Geological Map of Portugal at 1:1 000 000, 3rd edition. National Laboratory of Energy and Geology, Lisbon.

Luo, Q., Zhong, N., Dai, N., Zhang, W., 2016. Graptolite-derived organic matter in the Wufeng-Longmaxi Formations (Upper Ordovician–Lower Silurian) of southeastern Chongqing, China: Implications for gas shale evaluation. Int. J. Coal Geol. 153, 87–98. https://doi.org/10.1016/j.coal.2015.11.014.

Macqueen, R.W., 1984. Introduction: Role of Organisms and Organic Matter in Ore Deposition. Procediments Symposia Association Canada and Mineral Association, Montreal, p. 890.

Maia, M., Moreira, N., Mirão, J., Noronha, F., Nogueira, P., 2019. Fluid inclusions study of Cu-rich deposits from Sousel-Barrancos metallogenic belt (Ossa-Morena Zone, Portugal). In: Mineralogic and Petrographic Protocol Abstract Series (ECROFI 2019), 10, p. 79.

Maia, M., Moreira, N., Vicente, S., Mirão, J., Noronha, F., Nogueira, P., 2020. Multi-stage fluid system responsible for ore deposition in the Ossa-Morena Zone (Portugal): constraints in cu-ore deposits formation. Geology of Ore Deposits 62 (6), 508–534. https://doi.org/10.1134/S1075701520060094.

Mateus, A., Matos, J.X., Rosa, C., Oliveira, V., 2003. Cu-Ores in Quartz-Carbonate Veins at Estremoz-Alandroal and Barrancos-Sto Aleixo Regions (Ossa-Morena Zone): A Result of Late-Variscan Hydrothermal Activity. VI National Congress of Geology, Lisbon (Portugal), pp. F90–F93.

Mateus, A., Munhá, J., Inverno, C., Matos, J., Martins, L., Oliveira, D., Jesus, A., Salgueiro, R., 2013. Mineralizações no sector português da Zona de Ossa-Morena. Geologia de Portugal. In: Dias, R., Araújo, A., Terrinha, P., Kullberg, J.C. (Eds.), Volume I - Geologia Pré-mesozóica de Portugal. Escolar Editora, pp. 577–615.

Matos, J.X., Filipe, A., 2013. Carta de Ocorrências Mineiras do Alentejo e Algarve, Escala 1:400 000. National Laboratory of Energy and Geology.

Matos, J.X., Rosa, C., 2001. Diagnóstico Preliminar de Minas Abandonadas - Área Sul. Internal Report IGM, 276 pp.

Maynard, J.B., Elswick, E.R., Hower, J.C., 2001. Reflectance of dispersed vitrinite in shales hosting Pb–Zn–Cu ore deposits in western Cuba: comparison with clay crystallinity. Int. J. Coal Geol. 47, 161–170. https://doi.org/10.1016/S0166-5162(01)00040-4.

Melchin, M.J., Sadler, P.M., Cramer, B.D., 2012. The Silurian Period. In: Gradstein, F.M., Ogg, J.G., Schmitz, M., Ogg, G.M. (Eds.), The Geologic Time Scale, 2, pp. 525–558.

Mendonça Filho, J.G., Gonçalves, P.A., 2017. Organic matter: concepts and definitions, chapter 1. In: Suárez-Ruiz, I., Mendonça Filho, J.G. (Eds.), Geology: Current and Future Developments. The Role of Organic Petrology in the Exploration of Conventional and Unconventional Hydrocarbon Systems, vol. 1. Bentham Science Publishers, United Arab Emirates, pp. 1–33.

Meyers, P.A., Pratt, L.M., Nagy, B., 1992. Geochemistry of metalliferous black shales. Chem. Geol. 99, 211 pp.

Moreira, N., Araújo, A., Pedro, J.C., Dias, R., 2014. Evolução geodinâmica da Zona de Ossa-Morena no contexto do SW Ibérico durante o Ciclo Varisco. Comunicações Geológicas 101 (special volume I), 275–278.

Moreira, N., Pedro, J., Santos, J.F., Araújo, A., Dias, R., Ribeiro, S., Romão, J., Mirão, J., 2019. $^{87}Sr/^{86}Sr$ applied to age discrimination of the Palaeozoic carbonates of the Ossa-Morena Zone (SW Iberia Variscides). Int. J. Earth Sci. 108 (3), 963–987.

Mossman, D.J., 1999. Carbonaceous substances in mineral deposits: implications for geochemical exploration. J. Geochem. Explor. 66, 241–247.

Oliveira, V., 1984. Contribuição para o conhecimento geológico-mineiro da região Alandroal-Juromenha (Alto Alentejo). In: Studies, Notes and Works. Mining Development Services, Lisbon, XXVI, 1-4, pp. 103–126.

Oliveira, V., 1986. Prospecção de Minérios Metálicos a Sul do Tejo 1. In: Geosciences, pp. 15–22. Chapters 1-2.

Pasava, J., Kříbek, B., Vymazalová, A., Sýkorová, I., Žák, K., Orberger, B., 2008. Multiple sources of Metals of Mineralization in lower Cambrian Black Shales of South China: evidence from Geochemical and Petrographic Study. Resour. Geol. 58, 25–42. https://doi.org/10.1111/j.1751-3928.2007.00042.x.

Perdigão, J.C., Oliveira, J.T., Ribeiro, A., 1982. Explanatory Notice of Sheet 44-B (Barrancos) of the Geological Map of Portugal at Scale 1:50 000. Geological Surveys of Portugal.

Pereira, M.F., Silva, J.B., Chichorro, M., Ordóñez-Casado, B., Lee, J.K.W., Williams, I.S., 2012. Early Carboniferous wrenching, exhumation of high-grade metamorphic rocks and basin in-stability in SW Iberia: constraints derived from structural geology and U-Pb and ^{40}Ar-^{39}Ar geochronology. Tectonophysics 558-559, 28–44. https://doi.org/10.1016/j.tecto.2012.06.020.

Peters, K.E., Walters, C.C., Moldowan, J.M., 2005. The Biomarker Guide, 2nd edition. Cambridge University Press. https://doi.org/10.1017/S0016756806212056. 1155 pp.

Petersen, H.I., Schovsbo, N.H., Nielsen, A.T., 2013. Reflectance measurements of zooclasts and solid bitumen in lower Paleozoic shales, southern Scandinavia: Correlation to vitrinite reflectance. Int. J. Coal Geol. 114, 1–18. https://doi.org/10.1016/j.coal.2013.03.013.

Pi, D.H., Jiang, S.Y., Luo, L., Yang, J.H., Ling, H.F., 2014. Depositional environments for stratiform witherite deposits in the lower Cambrian black shale sequence of the Yangtze Platform, southern Qinling region, SW China: evidence from redox-sensitive trace element geochemistry. Palaeogeogr. Palaeoclimatol. Palaeoecol. 398, 125–131. https://doi.org/10.1016/j.palaeo.2013.09.029.

Piçarra, J.M., 2000. Estudo estratigráfico do sector de Estremoz - Barrancos, Zona de Ossa Morena, Portugal. PhD thesis,, Volume I and II, 268 pp.

Pohl, W.L., 2011. Economic Geology Principles and Practice. Wiley Blackwell John Wiley and Sons, New York, p. 688.

Quesada, C., Oliveira, J.T., 2019. The geology of iberia: a geodynamic approach. In: The Variscan Cycle, Volume 2. Springer International Publishing, 544 pp.

Ribeiro, A., Munhá, J., Dias, R., Mateus, A., Pereira, E., Ribeiro, M.L., Fonseca, P., Araújo, A., Oliveira, T., Romão, J., Chaminé, H., Coke, C., Pedro, J., 2007. Geodynamic evolution of SW Europe Variscides. Tectonics 26, TC6009. https://doi.org/10.1029/2006TC002058.

Rimmer, S.M., 2004. Geochemical paleoredox indicators in Devonian-Mississippian black shales, Central Appalachian Basin (USA). Chem. Geol. 206, 373–391. https://doi.org/10.1016/j.chemgeo.2003.12.029.

Robardet, M., Gutiérrez-Marco, J.C., 2004. The Ordovician, Silurian and Devonian sedimentary rocks of the Ossa-Morena Zone (SW Iberian Peninsula, Spain). J. Iber. Geol. 30, 73–92.

Robb, L.J., 2005. Introduction to Ore-Forming Processes. Blackwell Science Ldt, 373 pp.

Roseiro, J., Moreira, N., Nogueira, P., Maia, M., Araújo, A., Pedro, J., 2020. Depositional environment and passive-to-active margin transition as recorded by trace elements chemistry of lower-middle Palaeozoic detrital units from the Ossa-Morena Zone (SW Iberia). Geol. Communicat. 107 (II), 39–46.

Ross, D.J.K., Bustin, R.M., 2006. Sediment geochemistry of the lower Jurassic Gordondale Member, northeastern British Columbia. Bull. Can. Petrol. Geol. 54, 337–365.

Ross, D.J.K., Bustin, R.M., 2009. Investigating the use of sedimentary geochemical proxies for paleoenvironment interpretation of thermally mature organic-rich strata: examples from the Devonian-Mississippian shales, Western Canadian Sedimentary Basin. Chem. Geol. 260, 1–19. https://doi.org/10.1016/j.chemgeo.2008.10.027.

Schermerhorn, L.J.G., Priem, H.N.A., Boelrijk, N.A.I.M., Hebeda, E.H., Verdurmen, E.A. T., Verschure, R.H., 1978. Age and Origin of the Messejana Dolerite Fault-Dike System (Portugal and Spain) in the Light of the opening of the North Atlantic Ocean. J. Geol. 86 (3), 299–309. https://doi.org/10.1086/649692.

Semtner, A.K., Klitzsch, E., 1994. Early Paleozoic paleogeography of the northern Gondwana margin: new evidence for Ordovician-Silurian glaciation. Geol. Rundsch. 83, 743–751. https://doi.org/10.1007/BF00251072.

Shaw, T.J., Geiskes, J.M., Jahnke, R.A., 1990. Early diagenesis in differing depositional environments: the response of transition metals in pore water. Geochim. Cosmochim. Acta 54, 1233–1246. https://doi.org/10.1016/0016-7037(90)90149-F.

Sillitoe, R.H., 2005. Supergene oxidized and enriched porphyry copper and related deposits. Econ. Geol. 100, 723–768.

Silva, E.A., Miranda, J.M., Luis, J.F., Galdeano, A., 2000. Correlation between the Palaeozoic structures from West Iberian and Grand Banks margins using inversion of magnetic anomalies. Tectonophysics 321, 57–71. https://doi.org/10.1016/S0040–1951(00)00080–9.

Suárez-Ruiz, I., Flores, D., Mendonça Filho, J.G., Hackley, P.C., 2012. Review and update of the applications of organic petrology: part 2, Geological and Multidisciplinary applications. Int. J. Coal Geol. 98, 73–94. https://doi.org/10.1016/j.coal.2012.03.005.

Swaine, D.J., 1990. Trace Elements in Coal. Butterworths, London, p. 278.

Taylor, G.H., Teichmuller, M., Davis, A., Diessel, C.F.K., Littke, R., Robert, P., 1998. Organic Petrology. Gebrüder Borntraeger, Berlin, p. 704.

Tissot, B., Welte, D.H., 1984. Petroleum Formation and Occurrence, 2nd edition. Springer-Verlag, Heidelberg, p. 669.

Tornos, F., Inverno, C.M.C., Casquet, C., Mateus, A., Ortiz, G., Oliveira, V., 2004. The metallogenic evolution of the Ossa-Morena Zone. J. Iber. Geol. 30, 143–181.

Tribovillard, N., Algeo, T.J., Lyons, T., Riboulleau, A., 2006. Trace metals as paleoredox and paleoproductivity proxies: an update. Chem. Geol. 232, 12–32. https://doi.org/10.1016/j.chemgeo.2006.02.012.

US - EPA, 2002. Methods for the determination of Total Organic Carbon (TOC) in soils and sediments. In: United States Environmental Protection Agency (U. S. EPA), Office of Research and Development, National Exposure Research Laboratory, Las Vegas, NV. NCEA-C-1282, EMASC-001, 26 pp.

Velasco, F., Herrero, J.M., Suárez, S., Yusta, I., Alvaro, A., Tornos, F., 2013. Supergene features and evolution of gossans capping massive sulphide deposits in the Iberian Pyrite Belt. Ore Geol. Rev. 53, 181–203. https://doi.org/10.1016/j.oregeorev.2013.01.008.

Vine, J.D., Tourtelot, E.B., 1970. Geochemistry of black shale deposits - a summary report. Econ. Geol. 65, 253–272. https://doi.org/10.2113/gsecongeo.65.3.253.

Wang, Y., Chen, J., Shen, W., Li, Min, 2022. Mechanism of Organic Matter Accumulation in Black Shales of the Yuertusi Formation in the Tarim Basin: Insights from Paleoenvironmental Variation during the early Cambrian. Front. Earth Sci. 10 https://doi.org/10.3389/feart.2022.879658.

Wignall, P.B., 1994. Black Shales. Clarendon Press, Oxford, England, p. 127.